ACS NANO

Open Access

www.acsnano.org

REVIEW

Design Chemical Exchange Saturation Transfer Contrast Agents and Nanocarriers for Imaging Proton Exchange *in Vivo*

Haoyun Su and Kannie W. Y. Chan*

Cite This: *ACS Nano* 2024, 18, 33775–33791

Read Online

ACCESS | Metrics & More | Article Recommendations

ABSTRACT: Chemical exchange saturation transfer magnetic resonance imaging (CEST MRI) enables the imaging of many endogenous and exogenous compounds with exchangeable protons and protons experiencing dipolar coupling by using a label-free approach. This provides an avenue for following interesting molecular events *in vivo* by detecting the natural protons of molecules, such as the increase in amide protons of proteins in brain tumors and the concentration of drugs reaching the target site. Neither of these detections require metallic or radioactive labels and thus will not perturb the molecular events happening *in vivo*. Yet, magnetization transfer processes such as chemical exchange and dipolar coupling of protons are sensitive to the local environment. Hence, the use of nanocarriers could enhance the CEST contrast by providing a relatively high local concentration of contrast agents, considering the portion of the protons available for exchange, optimizing the exchange rate, and utilizing molecular interactions. This review provides an overview of these factors to be considered for designing efficient CEST contrast agents (CAs), and the molecular events that can be imaged using CEST MRI during disease progression and treatment, as well as the nanocarriers for drug delivery and distribution for the evaluation of treatments.

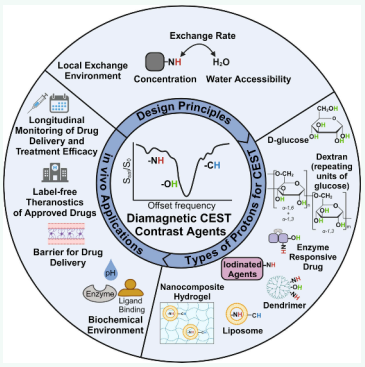

KEYWORDS: *CEST, MRI, molecular imaging, contrast agent, nanocarrier, theranostics, drug delivery, nanomedicine, chemotherapeutics, liposome, hydrogel*

1. INTRODUCTION

Contrast enhanced imaging is essential for the identification of abnormalities and pathologies *in vivo*. Among the clinical imaging modalities, such as computed tomography (CT), positron emission tomography (PET), and magnetic resonance imaging (MRI), MRI is the only noninvasive imaging modality that does not require ionizing radiation or radioactive tracers. Gadolinium-based contrast agents (GBCAs) have been used for tens of millions of MRI sessions every year.[1] However, nephrogenic systemic fibrosis has been found in renal-compromised patients with frequent MRI examinations using GBCAs, especially those GBCAs that have relatively low stability where gadolinium ions could leak out and accumulate in the body.[2] Thus, there is a need to detect key events or molecular events that are necessary for the diagnosis and monitoring of therapies without the use of metallic and radioactive agents. Therefore, chemical exchange saturation transfer (CEST) MRI has shown promises in the identification of tumor recurrence from radiation necrosis based on the protein content *in vivo* using the amide proton exchange.[3−6] Since CEST detects proton exchange, which is inherently very pH-sensitive, it enables the detection of the penumbra region in stroke based on pH maps using CEST contrast.[7−9] Moreover, many approved drugs have exchangeable protons that can be detected by CEST without the need to add metallic labels (a label-free approach).[10] Overall, CEST MRI provides valuable information about the proton exchange *in vivo*, either using endogenous molecules or exogenous molecules with protons for CEST. These molecular events would not be easily detected by other imaging modalities, especially in a totally noninvasive manner.

The study of proton exchange can provide insights into the conformational and dynamic properties of macromolecules, especially proteins and their interactions *in vivo*.[11−13] Traditionally, proton nuclear magnetic resonance (^{1}H NMR) is used to detect the presence of exchangeable protons using the D_2O

Received: May 5, 2024
Revised: August 29, 2024
Accepted: September 6, 2024
Published: December 6, 2024

spectrum of molecules or using a water exchange filter (WEX) in phantoms.[14] CEST has rapidly emerged as a powerful MR imaging technique to detect proton since it was reported by Ward and Balaban in 2000.[15] Its contrast originates from the continuous transfer of magnetization between frequency-selective irradiated protons and bulk water protons. When exchangeable protons are irradiated with a radio frequency (RF) pulse, they can transfer this saturation to water through chemical exchange (Figure 1A (i)). Additionally, such

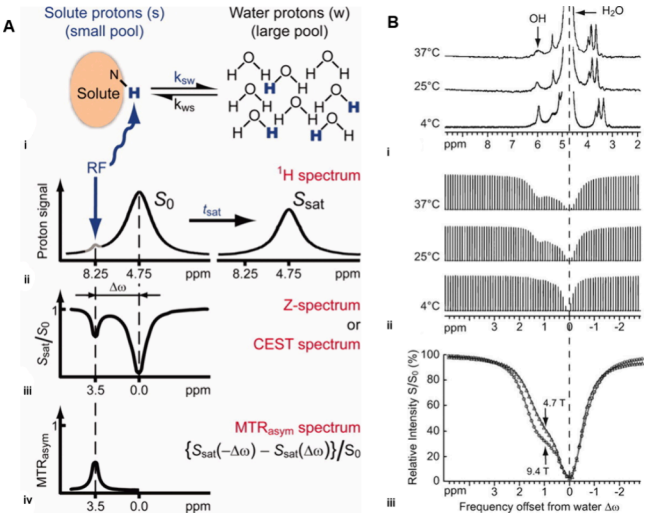

Figure 1. CEST and its relation to ^{1}H NMR. (A) Mechanism of CEST contrast generation. i: Solute protons are saturated with radiofrequency irradiation at their resonance frequency, and the saturation is transferred to bulk water protons, while unsaturated protons return to the solute pool. ii, iii: with a repeated process of exchanging saturation, the CEST effect becomes visible on ^{1}H-spetrum/Z-spectrum at the proton's resonance frequency ($\Delta\omega$). iv: MTR$_{asym}$ is an analysis method of the Z-spectrum to remove the direct saturation effect of water (MTR$_{asym}$ = $S_{sat}(-\Delta\omega)/S_0 - S_{sat}(\Delta\omega)/S_0$). (B) Glycogen with exchangeable hydroxyl groups measured with ^{1}H NMR (i) and CEST (ii) at various temperatures in water. An elevated exchange rate caused by the increasing temperature made the glycogen proton signal less visible, while the CEST signal was more detectable. iii: Fast-exchanging glycogen in PBS is more detectable at higher field strength due to higher saturation efficiency. Reprinted with permission from ref 18. Copyright 2011 John Wiley & Sons.

saturation transfer could also happen in RF-irradiated nonexchangeable protons that engage in through-space dipolar coupling with nearby protons. The coupled protons undergo cross-relaxation, where the saturation is transferred to bulk water.[16] Chemical exchange and cross-relaxation could be major components of the relaxation mechanism in biological tissue in magnetization transfer experiments *in vivo*, and the exchange between water and a series of metabolites and exogenous diamagnetic compounds could then be measured by CEST.[15,17] With the repeated saturation transfer, this saturation effect will be detected as the reduction of bulk water signal over a series of offset frequency at steady state, hence the name Z-spectrum (Figure 1A (ii-iii)).[18] Notably, the water resonance frequency is at 0 ppm in CEST experiments, in contrast to that at 4.7 ppm in NMR. Although CEST shares many similarities with NMR, factors such as temperature could affect CEST and NMR spectra differently, as one is detecting the exchange environment while the other is detecting the chemical environment. The example of detecting glycogen (Figure 1B) demonstrates such a difference. Exchange rate increased when the temperature increased, thus resulting in an excessive broadening of exchangeable hydroxyl proton signal in NMR (Figure 1B (i)). While in CEST experiments (Figure 1B (ii-iii)), by measuring the water signal, hydroxyl protons of glycogen were readily detected.[18] Given its contrast mechanism, CEST is well-suited for label-free detection of a wide range of endogenous and exogenous compounds where the labile protons such as hydroxyl, amine, and amide protons are exchanging at a slow-to-intermediate rate on an NMR time scale.[18]

Many endogenous molecules can be detected by CEST. For example, amide proton transfer (APT) has shown success in evaluating tumor grading, metabolism, genetic mutation status, progression and recurrence, response to treatment, and has gained FDA approval for the clinical use of molecular assessment of brain tumors.[4,5,19−22] Glutamate-weighted CEST contrast has been detected in the brain and neurological disorders.[23,24] The guanidinium protons of creatine in the brain and muscle can be imaged, indicating the molecular kinetics.[25−29] Hydroxyl protons of sugar molecules, which are a major category of biomolecules, can be detected via CEST and serve as disease biomarkers indicating molecular alterations in the brain, in tumors at multiple locations, in organs, and in the knee.[30−34] Non-exchangeable aliphatic protons can be detected in CEST experiments, where saturation is transferred via cross-relaxation and eventually relayed to bulk water, namely the relayed nuclear Overhauser enhancement (rNOE).[16] With both rNOE and CEST being different processes under magnetization transfer, they can be monitored simultaneously on the downfield and upfield sides of Z-spectra in CEST experiments. In addition to the rNOE signals observed in proteins that are assigned to the side chains, rNOE has been observed in organized structures such as cell membranes and liposomes, presumably originated from the choline component or the aliphatic protons of lipid molecules.[35,36] Many studies have been devoted to developing fast and accurate acquisition and post-processing methods for decoupling other confounding effects *in vivo* CEST signals and extracting essential information for diagnosis and treatment evaluation.[37−39]

Exogenous CEST detectable compounds are widely exploited as CEST contrast agents (CEST CAs), further aiding disease diagnosis and treatment monitoring. Compared with traditional gadolinium-based contrast agents and iron-based T_2 contrast agents, exogenous nonmetallic CEST CAs have the advantages of high biocompatibility, the ability to report on the molecular environment, and rapid translation to the clinic. CEST CAs can be in the form of standalone molecules, CEST-detectable carriers, or a combination of both. They can be categorized based on size, structure, modes of exchange, and the molecular events they are intended to probe. Several excellent review articles have discussed CEST CAs from various perspectives, such as the nature of the molecule, type of the carrier, and application in specific diseases.[10,40−50] Furthermore, through careful selection and design of CEST CAs, it is possible to obtain CAs with desirable properties, including robust and stable CEST signals, and additional insights into molecular interactions and alterations. This can be achieved by choosing adequate CEST CAs with suitable exchange and physicochemical properties to effectively generate the desired contrast. In this review, we discuss how the characteristics of CEST CAs determine their detectability

https://doi.org/10.1021/acsnano.4c05923
ACS Nano 2024, 18, 33775−33791

of distinct proton exchanges, focusing on the nanocarrier design aspect. This includes design criteria for exogenous CEST CAs to maximize their CEST contrast efficiency, followed by *in vivo* applications of non-metallic CEST CAs with a focus on their local exchange environments and molecular interactions. Further information about the CEST mechanisms and technical aspects can be found in recent reviews.[37,38,50−66]

2. DESIGN CONSIDERATIONS FOR AN EFFICIENT CEST CA

The detectability of CEST CAs is determined by the physicochemical properties of the molecules and their interactions with the local environment of the nanocarriers *in vivo*. By understanding the properties of exchangeable protons and their local environment, acquisition parameters such as irradiation power and saturation duration could then be optimized, which have been reviewed elsewhere.[37,38,52,67] Here we will focus on several factors that can be optimized through CEST CA design and therefore directly modulate the CEST contrast generated. An illustration of how the interplay of these CEST factors could guide the design of CEST CA systems is shown in Scheme 1B.

2.1. Local Concentration of CEST CA. One primary motivation for designing CEST CAs is to increase the number of magnetically equivalent protons for CEST detection to improve sensitivity,[71] especially for *in vivo* applications where confounding factors could attenuate the signal of CEST CAs of interest. It is important that the minimum concentration threshold for CEST detection should be met. Generally, the desirable concentration of exchangeable protons in small-molecule CEST CAs is around a few millimolar (10^{-4}−10^{-1} M).[18] The local concentration of protons can be increased by incorporating CEST CAs into nanocarriers. Liposome is a nanosized vesicle where the inner aqueous core is separated from surrounding bulk water with a semipermeable lipid bilayer. It remains the state-of-the-art for CEST CA system due to its ability to carry high payloads of agents within its inner core and increase the local drug concentration.[41,48] Small-molecule diamagnetic CEST CAs can be encapsulated into the liposome and generate CEST signals through proton exchange with intraliposomal water.[50] Nanomaterials with large numbers of functionalizable sites are also favorable. In particular, conjugation of small-molecule CEST CAs to dendrimers or carbon dots with large number of modifiable surface functional groups will also result in higher local concentration of exchangeable protons.[43,72−74] For example, the detection sensitivity could be further increased to hundreds of micromolar when small-molecule CEST CAs, such as salicylic acid, are conjugated to the dendrimer.[73] This detection sensitivity also depends on the properties of the nanocarriers, such as water accessibility and interaction between exchangeable protons.

Various clinically used therapeutic drugs and pharmaceutical excipients exhibit CEST effects originating from exchangeable moieties in their structure and could be directly utilized as theranostic CEST CAs.[10,46,75] Some less water-soluble anticancer drugs can still be detected by CEST.[10] A way to enhance their solubility and thus increase the concentration of protons available for exchange is to use solvent−water mixture systems with approved pharmaceutical excipient solvents, such as ethanol.[76] With the proper choice of solvent system, the solubility of sparsely soluble drugs could be increased by multiple-fold.[76−78] Moreover, it is recently reported that a series of commonly used polar solvents, including DMSO and ethanol, are detectable at negative offset frequencies down to 1.25% v/v concentration in water.[79] Therefore, it is feasible to simultaneously monitor the CEST signal of the drug with enhanced solubility and that of the solvent system at their respective offsets.

Scheme 1. (A) CEST CAs Enhance Contrasts at Distinct Offset Frequencies from the Exchange of Protons from −NH and −OH, and the Dipolar Coupling and Resulting Magnetization Transfer of −CH.[18,56] (B) A Schematic Nanocomposite Hydrogel Structure Demonstrating CEST Considerations in the Rational Design for a CEST Nanocarrier System[a]

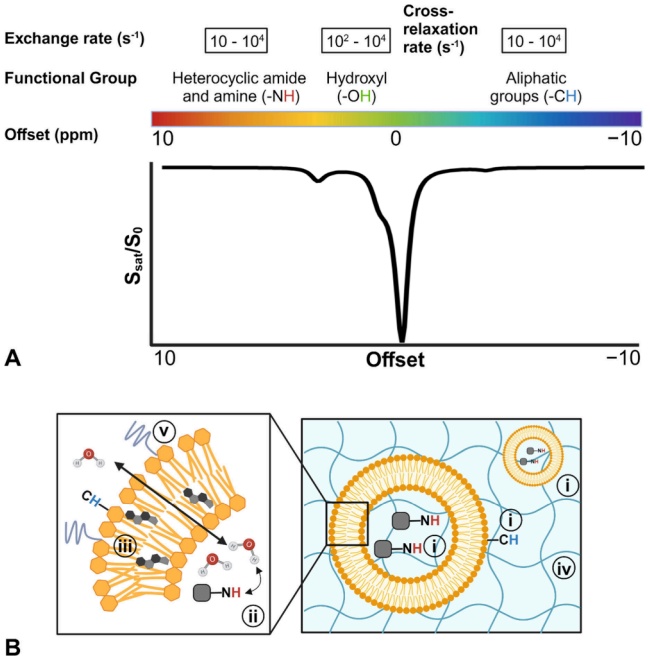

[a]i: Liposome carrying high payload of small-molecule CEST CAs boosts the local concentration of exchangeable protons, which is further maintained by incorporation into the hydrogel matrix.[68] Aliphatic protons from the phospholipid bilayer could offer additional contrast for monitoring the liposome.[35] ii, iii: Exchange rate is modulated by liposome size and lipid bilayer composition (headgroup, carbon chain length, degree of saturation, and cholesterol content) and therefore the water transfer across the bilayer.[68−70] iv: The local exchange environment including pH affects the observed contrast. v: Tunable surface properties such as charge and targeting moieties allow targeted delivery of the cargo. (Created with BioRender.com).

2.2. Exchangeable Proton Fraction. The portion of labile protons that participate in the exchange process can vary in response to the change in structure or conformation induced by the molecular environment. This characteristic has been exploited to develop CEST CAs that are sensitive to the local environment, where the CEST contrast of both drugs/agents and their products are examined. Enzymatic cleavage can expose functional groups that are previously not accessible to water and exchange process, or "deactivate" functional groups from generating CEST signal.[80−82] Several CEST CAs were designed based on this principle and are referred to as CatalyCEST. For example, Sinharay et al.[83] synthesized a compound with a cleavable sulfate group that masks the

https://doi.org/10.1021/acsnano.4c05923
ACS Nano 2024, 18, 33775−33791

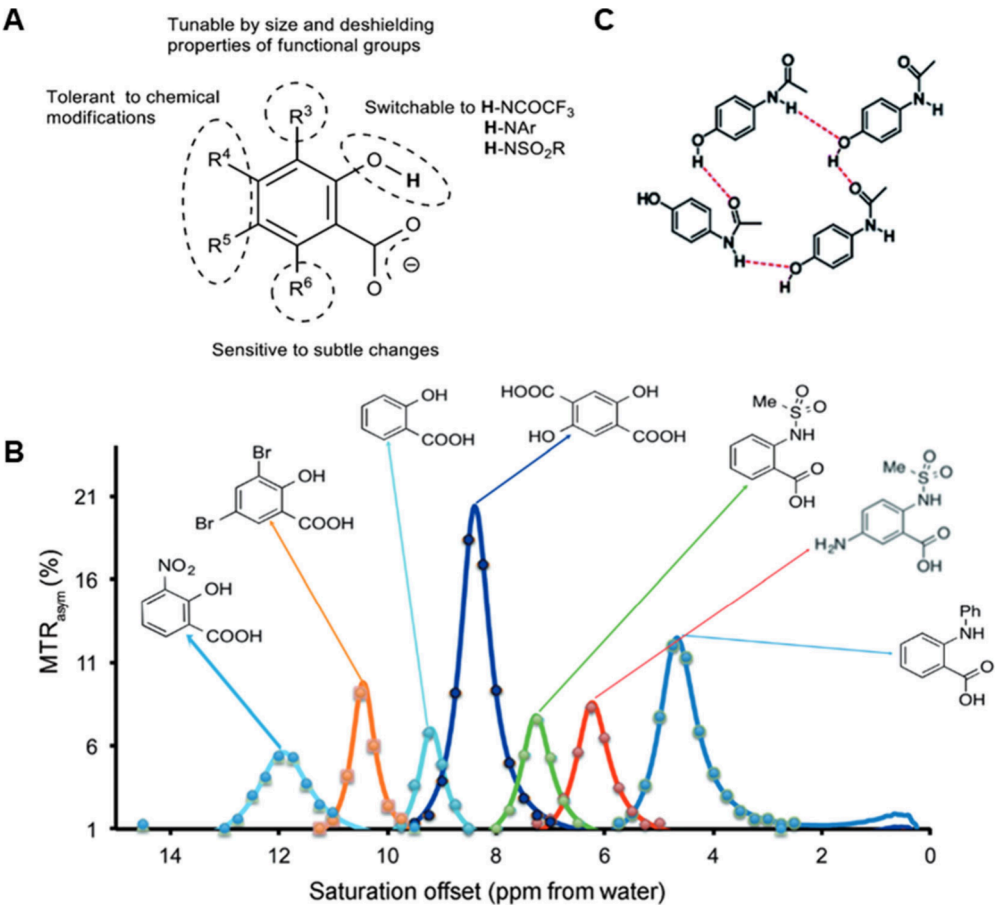

Figure 2. Chemical structure and interaction affect k_{ex} significantly. (A, B) Stereoelectronic effect on the CEST properties of phenol-based CEST agents, showing modification at different positions affect k_{ex} to different extents. Reprinted with permission from ref 95. Copyright 2014 John Wiley & Sons. (C) Illustration of the hydrogen-bonded sheet of paracetamol. Reprinted with permission from ref 96. Copyright 2021 The Authors. Published by the Royal Society of Chemistry.

salicylic acid moiety from producing CEST signal. By observing the appearance of a salicylic acid CEST signal, sulfatase enzyme activity can be indirectly monitored. With a similar concept, alkaline phosphatase enzyme, γ-glutamyl transferase, kallikrein 6, and cathepsin B activity were also detected by tailor-made CatalyCEST CAs.[84−87] For deactivation of CEST signal by enzyme, cytosine deaminase removes the amine group from both CEST-detectable cytosine and 5-fluorocytosine, catalyzing them into products that are not CEST-detectable.[88] Furthermore, deoxycytidine and its product deoxycytidine triphosphate that metabolized by deoxycytidine kinase, can be detected via CEST without synthetic labeling due to their exchangeable amine protons resonating at 2 ppm.[89] The activity of deoxycytidine kinase was then measured in leukemia cancer xenografts by monitoring the substrate and product. In addition to enzymes, aldehyde (byproduct of vitamin B6 metabolism)-conditional CEST CAs (termed HydrazoCEST) were also synthesized and demonstrated the ability to report the presence of aromatic aldehyde. CEST signal was generated upon the CEST CA undergoing hydrazone formation with aldehyde.[90]

The performance of CEST CAs *in vivo* is markedly influenced by the exchange environment convoluted by the magnetization transfer effects of various types of biomolecules. Proteins, a major category of biomolecule, exist in various states and perform biological functions determined by their structures. CEST MRI has demonstrated successes in detecting proteins with exchangeable amide groups.[3,91] Furthermore, unfolding and aggregation of proteins were also detected by exchange or NOE mediated CEST effect in heterogeneous mixture of protein solution.[92,93] Such conformational changes of protein would alter the accessibility of water, affecting both the detection of the protein CEST effect and the biodistribution of CEST CAs in the region. Therefore, taking this altered exchanging fraction into account can guide the design of effective conformation-sensitive CEST CA for assessing protein pathology in neurodegenerative diseases, including Alzheimer's disease (AD) and Parkinson's disease (PD), where structurally diverse proteins are present.[94]

2.3. Exchange Rate. The exchange rate (k_{ex}) of CEST CAs has multiple determinants, from the structure of the CA, the type of carriers the CA associates with, and the exchange environment. According to CEST theory, k_{ex} of the protons should not exceed its frequency offset (i.e., $\Delta\omega \geq k_{ex}$) in order to generate the CEST signal. The study on phenolic compounds serves as a good example of how phenol-based analogs with different chemical structures can have drastically different offset frequencies and k_{ex} due to different stereoelectronic effects experienced by exchangeable protons (Figure 2A-B).[95] Moreover, intramolecular and intermolecular hydrogen bonding also modulate k_{ex}. Paracetamol, a common analgesic drug, falls into the CEST-detectable range due to its intermolecular hydrogen-bonded sheet structure (Figure 2C).[96] To facilitate the development of clinical applications

https://doi.org/10.1021/acsnano.4c05923
ACS Nano 2024, 18, 33775−33791

for CEST CAs, k_{ex} also needs to accommodate the common clinical field strength at 3 T and an irradiation power within the specific absorption rate (SAR).[15,52]

In addition to hydrogen bonding, the pH also plays a crucial role in the resulting k_{ex}. This could be exploited as a strategy to modulate k_{ex} and render the exchanging moieties detectable. For example, hydroxyl protons have an exchange rate at about 2300 s^{-1} at pH 7.3, which belongs to the fast exchange regime and could have attenuated CEST signal at physiological pH, but enhanced contrast at acidic tumor microenvironment due to reduced k_{ex}.[97,98] A thymidine-based compound is used as a CEST imaging probe for herpes simplex virus type-1 thymidine kinase, where optimal k_{ex} for the CEST CA was obtained when the pK_a increased.[99] Mapping pH *in vivo* could be performed using clinical iodinated CT agents iopamidol as well.[100,101] It has two peaks at 4.2 and 5.5 ppm originating from separate amide groups on the iopamidol molecule with different pH dependency. Therefore, by comparing the two peaks (the ratiometric approach), *in vivo* pH could be accurately mapped out with less influence by the concentration effect. Meanwhile, CT agents with a single amide group can detect pH changes as well since the CEST signal depends on the exchange rate and saturation parameters, such as the irradiation power, allowing another ratiometric approach for measuring pH.[102] This has led to successful pH mapping with CT agents in preclinical disease models and healthy volunteers.[103−105]

Utilization of nanocarriers could further improve CEST contrast efficiency by modulating k_{ex}. For example, glucose encapsulated in liposomes of different formulations demonstrated a decrease of k_{ex} to different extents, highly related to lipid bilayer permeability.[70] Dextran, a polysaccharide composed of repeating glucose units, are present in different molecular weights with abundant hydroxyl groups generating contrast at around 1 ppm.[106] k_{ex} of dextran is also pH-dependent like that of glucose, with a rapid k_{ex} of ∼3000 s^{-1} at pH 7.0 and turning into slow-to-medium regime at lower pH.[98] These characteristics have made dextran suitable for detecting heterogeneous and acidic tumor environments.

Since the principle of CEST is the detection of the magnetization transfer between solute protons and bulk water, k_{ex} would be an important determinant for generating CEST contrast. An effective CEST CA should have its k_{ex} within a detectable range and be optimized for saturation and acquisition parameters according to the field strength, including the irradiation power and saturation duration. This will depend on the specific application as well. For example, the molecule of interest in an acidic tumor microenvironment could be more detectable than at physiological pH; thus, the local exchange environment including the biochemical environment of the physio-/pathological processes must be considered.[97] The range of exchange rate for different chemical groups is given in Scheme 1A. Ideally, k_{ex} of the CA should be in slow-to-intermediate range, considering all the constraints from acquisition, *in vivo* environment, and nanocarriers. As shown in Figure 1B (ii), with lower k_{ex} (at 4 °C), the glycogen signal is less prominent on the Z-spectrum. While increasing k_{ex}, it becomes more detectable. However, if k_{ex} continues increasing, then the glycogen peak will coalesce with the water peak and become no longer detectable. Acquisition and quantification methods to identify the contribution of exchanging species with distinct k_{ex} properties are extensively studied by researchers as well.[52,107,108]

In addition to CEST, other MRI methods sensitive to chemical exchange have been used to detect molecules at certain k_{ex} range.[66] Saturation with frequency alternating RF irradiation (SAFARI) acquires a series of images to remove confounding magnetization transfer effects and measure exchange rates smaller than 200 s^{-1}.[109] Another approach is the variable delay multipulse (VDMP) that acquires two VDMP images to detect molecules at k_{ex} < 100−150 s^{-1} (slow-to-intermediate) in a sensitive manner.[110] Spin-lock imaging applies a spin-locking RF pulse to select protons exchanging at a specific k_{ex}. It is sensitive to slow k_{ex} when the spin-lock is applied at offset frequencies other than that of water at 0 ppm, which has been applied to detect endogenous slow exchanging amide protons. When it is applied at the water resonance frequency, intermediate exchanging hydroxyl and amine protons can be detected.[111]

2.4. Molecular Motion and Interactions. Magnetization transfer can be achieved through different pathways. Small molecules that experience transient binding can participate in the pathway and lead to the buildup of a pronounced magnetization transfer effect. Macrocyclic-based nanocarriers and liposomes play a crucial role in ^{129}Xe HyperCEST to ensure a sufficient amount of trapped xenon, an adequate dissociation rate and exchange rate for CEST detection.[112]

Detection of small biomolecules can be achieved by a CEST-based method that is sensitive to molecular binding. IMMOBILISE (IMaging of MOlecular BInding using Ligand Immobilization and Saturation Exchange) established a two-step approach that involves the magnetization transfer from −CH protons of mobile ligand in bound state to target exchangeable protons and subsequently to bulk water through chemical exchange. With repeated transfer through the target and eventually to water, signal reduction (saturation) on the water signal could be observed (Figure 3).[113,114] Since the

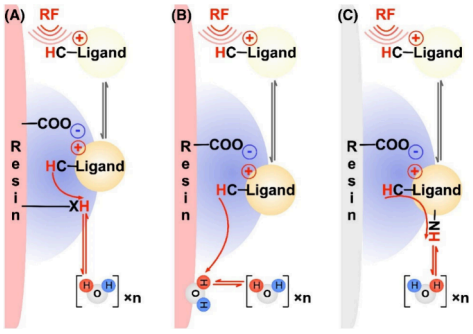

Figure 3. Possible pathways for the NOE-based saturation transfer of small-molecules undergoing electrostatic binding. Upon binding to an immobilized resin, RF-labeled aliphatic protons could transfer saturation intermolecularly to exchangeable protons on the resin or to bound water (A, B) through spin-diffusion, then to free water. The third pathway would be RF-labeled protons transfer saturation intramolecularly to exchangeable protons on the ligand and subsequently to water (C). Reprinted with permission from ref 114. Copyright 2022 John Wiley and Sons.

IMMOBILISE signal is sensitive to weak to moderate (10^1 to 10^{-7} M) binding affinity which is biologically relevant, biomolecular interactions could be detected by this method. For example, the binding of caffeine in rodent brain was detected with IMMOBILISE.[113]

In addition to biomolecules, biologically relevant ions (such as Ca^{2+}) can be detected using ^{19}F-CEST. Through the

https://doi.org/10.1021/acsnano.4c05923
ACS Nano 2024, 18, 33775−33791

binding kinetics of Ca^{2+}, the magnetically labeled Ca-5F-BAPTA (Ca^{2+} bound ^{19}F chelate) could transfer saturation to free 5F-BAPTA, resulting in a reduction of ^{19}F signal at 5 ppm.[115] Furthermore, detection of Zn^{2+} and Fe^{2+} at their respective offsets can be achieved simultaneously with a modified chelate, i.e., tetrafluorinated BAPTA (TF-BAPTA).[116]

3. LABEL-FREE IMAGING OF MOLECULAR EVENTS *IN VIVO*

Along with the rapid development of CEST MRI for the label-free imaging of biomolecules with protons for CEST, there are a few hurdles to overcome. Most endogenous biomolecules have functional groups exchanging at a range of 4 to −4 ppm offset frequencies. Overlapping signals could make CEST effects challenging to interpret, especially for offsets that are close to the water peak. In addition, the complex exchange environment *in vivo* could be an obstacle to the extraction of CEST signals from molecules of interest. Thus, tailored CA design, CEST acquisition, and postprocessing need to be considered for *in vivo* applications. CEST CAs with different sizes and architectures provide various advantages for the detection of a series of molecular activities. Small-molecule standalone CEST CAs, nanoparticle incorporated CEST CAs, and nanocomposite hydrogel based CEST CAs will be separately discussed and supplemented by their *in vivo* applications.

3.1. Imaging Biological Processes by Enhanced CEST Contrast via Compartmentalization. CEST detects the distribution of small molecules *in vivo*. Natural D-glucose and dextran of various molecular weight are utilized to study glucose metabolism (Figure 4A) and vascular permeability (Figure 4B), since their biodistribution is determined by perfusion, uptake and utilization.[97,106,117,118] The different uptake and utilization of D-glucose in tumors with different aggressiveness could be detected by glucoCEST (Figure 4A). Moreover, CT agents can be repurposed as CEST pH agents such as iopamidol. By accessing the CEST contrast of iopamidol at two offset frequencies, pH maps can be generated to differentiate between normal and injured kidneys (Figure 4C).[101] Some small-molecule CAs have CEST signals further away from common endogenous molecules. Barbituric acid and salicylic acid have CEST signal at 5 ppm and around 9 ppm respectively, which make them less overlapped with endogenous signals.[119,120]

The use of nanocarriers has multifold benefits, including tunable size and physicochemical properties, and controlled release of the cargo. Importantly, CEST CA loaded nanocarriers provide a relatively high local concentration, prolonged circulation, and increased affinity/preferential accumulation at the target site. An example illustrating the beneficial role of the nanocarrier is glucose and dextran. With comparable CEST properties (Section 2.3), dextran can serve as a nanocarrier containing multiple glucose units, providing a high local concentration of hydroxyl protons (e.g., Dex1 with 6 glucose units has 6 times more protons than glucose per molecule), and it exhibited a relatively longer circulation time compared to glucose.[98] In Figure 4B, dextran of 70 kDa had enhanced retention than that of 10 kDa dextran, providing a longer time window for imaging.[97,106] By conjugating prostate-specific membrane antigen (PSMA) onto dextran, it can target PSMA expressing tumors.[121]

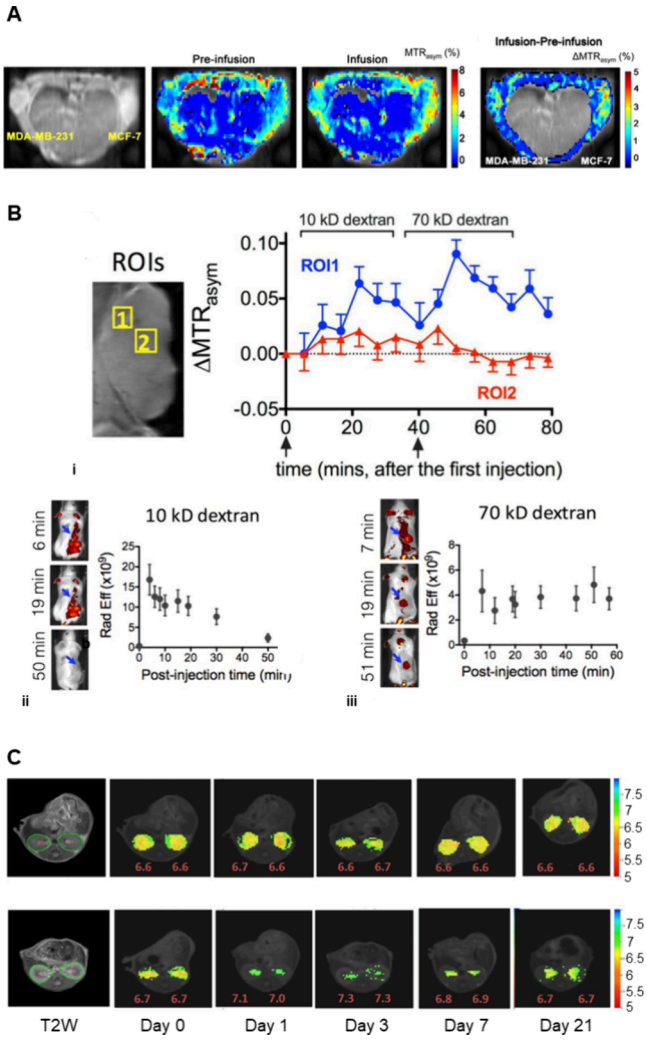

Figure 4. Biodistribution of small-molecule CEST CAs. (A) Natural D-glucose with hydroxyl groups injected into two mice bearing MDA-MB-231 and MCF breast tumors. By subtracting CEST map after D-glucose infusion from that of before, different levels of glucoCEST signals were observed at each tumor region, suggesting contribution from enlarged extravascular and extracellular space (EES) and its acidic environment. Reprinted with permission from ref 97. Copyright 2012 John Wiley and Sons. (B) i: Dextran of 10 and 70 kDa were injected to mice with subcutaneous tumor, and CEST imaging was done at several time points after injection. ii, iii: Fluorescence imaging validation for CEST peaks shown in panel i that could originate from the size-dependent dextran uptake by tumor. Reprinted with permission from ref 106. Copyright 2017 John Wiley and Sons. (C) pH maps obtained with the ratiometric CEST approach using iopamidol overlaid on kidney anatomical images (top row: control group; bottom row: AKI injection group) on various time points. Dynamic processes of the rapid pH increase peaked at Day 3 of AKI and the subsequent lowering of pH were imaged with CEST. Reprinted with permission from ref 101. Copyright 2012 John Wiley and Sons.

Besides dextran, liposomes and dendrimers are also utilized to increase the local concentration and achieve preferential accumulation. In Figure 5B, CEST detectable neuroprotectant citicoline was loaded into liposome decorated with polyethylene glycol (PEG) and vascular cell adhesion molecule 1 (VCAM-1) targeting moieties and achieved targeted delivery to lesion with label-free imaging of the delivery.[122] Monitoring

https://doi.org/10.1021/acsnano.4c05923
ACS Nano 2024, 18, 33775−33791

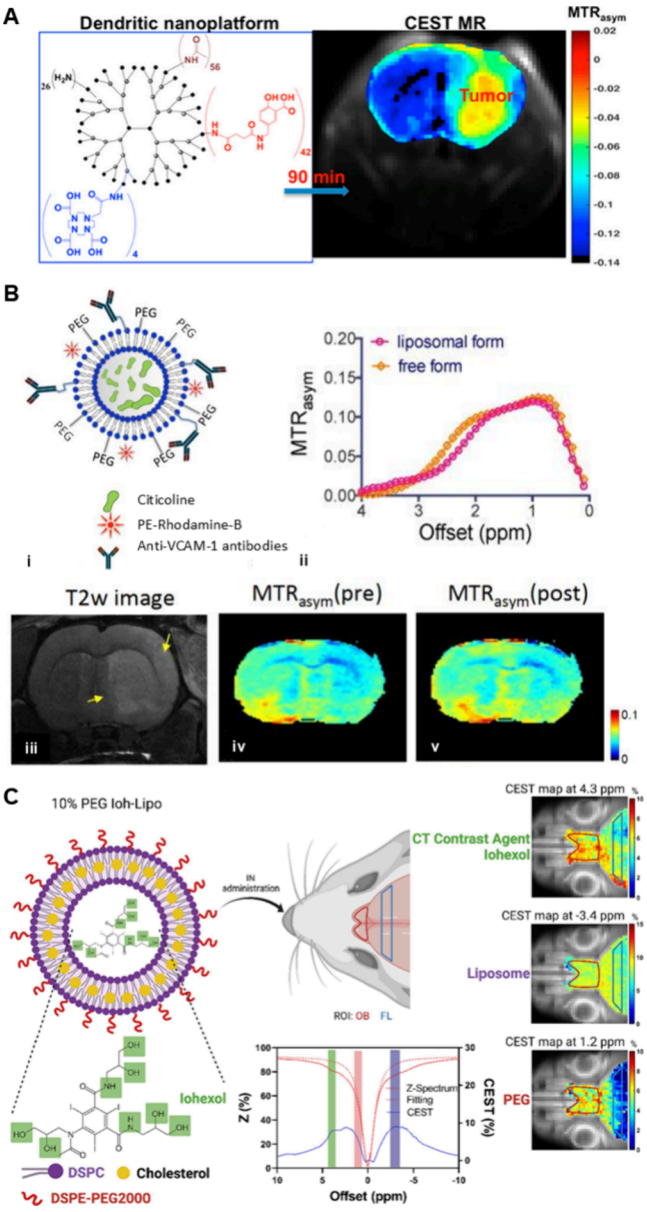

Figure 5. CEST CAs in the nanoparticle form. (A) Salicylic acid conjugated to dendrimer greatly increased the number of exchangeable protons and showed enhanced contrast at the tumor region. Reprinted with permission from ref 73. Copyright 2016 American Chemical Society. (B) VCAM-1 targeting liposome encapsulating citicoline as a theranostic agent. i, ii: Schematic diagram and CEST measurements of citicoline liposome. iii-v: T_2 image of the ischemic lesion, and CEST parametric map (MTR_{asym}) of the brain before the liposome injection and after 1.5 h of injection showed preferential accumulation at the ischemic lesion in rat brain. Reprinted under CC BY-NC License from ref 122. Copyright 2016 Ivyspring International Publisher. (C) Mucus-penetrating liposome encapsulating CEST detectable iohexol and its intranasal delivery to the olfactory bulb and frontal lobe could be imaged. Reprinted with permission from ref 123. Copyright 2023 Elsevier.

of mucus-penetrating liposome's delivery and accumulation via the nose-to-brain route is also feasible, with 10% PEG formulation of liposome and encapsulation of CT agent iohexol as an indicator (Figure 5C).[123] Dendrimers can also be fabricated to conjugate large amount of salicylic acid, achieving CEST detection at 500 μM dendrimer concentration, while retaining a high clearance rate due to ~5 nm size of dendrimer (Figure 5A).[73]

Nanocomposite hydrogels can serve as a platform for CEST CAs, allowing control over properties and functionalities of the multiparametric CEST CA system.[124,125] Incorporating small molecular CEST CAs into the nanocomposite hydrogel systems has multifold benefits in terms of offering a cleaner background with less endogenous molecules and controlled exchange environments for incorporated CAs, facilitating the controlled release, maintaining relatively high local concentration, and providing additional compartments for theranostic applications. Specifically, embedding pH nanosensors (i.e., L-arginine liposome-loaded hydrogel) enabled the detection of cell viability via imaging the concurrent decrease in pH when cell death occurred (Figure 6A).[68] In another study by Han et al.,[126] the small-molecule drug barbituric acid (BA) was encapsulated in liposomes, which were subsequently loaded into the alginate hydrogel matrix. In this nanocomposite hydrogel, multiple components could be detected using CEST MRI, indicating the relative concentrations of BA and liposome, respectively. Interestingly, distinctive release profiles were observed for BA and liposomes at their respective offsets (5 and −3.4 ppm) using CEST MRI (Figure 6B). Moreover, other types of hydrogels, such as gelatin and hyaluronic acid (HA), have a large number of exchangeable protons that could be detected by CEST (Figure 6C).[127,128]

There are many successful studies showing that CEST CAs, at either the free agent level or nanocarrier level, could be tailored to image specific physiological processes or diseases, as the exchange environments are specific combinations of various biological activities. While the above discussion provides an overview of the CEST CA design strategies illustrated by several key studies, there are many more studies employing thoughtfully designed CEST CAs that contribute valuable insights to the field of CEST MRI. These studies are not discussed in detail here but are comprehensively summarized in Table 1, which includes CEST CAs that are biochemically responsive (e.g., enzymatic activity, ligand binding, pH change), capable of crossing drug delivery barrier, and translating approved drugs into theranostic agents.

3.2. Imaging Drug Release and Distribution. Many clinically used drugs and compounds can be detected by CEST MRI using a label-free approach that facilitates theranostic applications.[10,46] For example, deoxycytidine kinase (DCK) is one of the enzymes clinically proven to be essential for the activation of a series of chemotherapeutics such as gemcitabine and is known to be associated with cancer resistance.[150] Advantageously, CEST detects DCK activity label-free by monitoring the accumulation of the product of the enzymatic conversion in tumor cells, where higher CEST contrast can be observed in DCK (+) tumor cells.[89]

Drug solution administered alone could be cleared by metabolism, renal, or hepatobiliary pathway,[151] resulting in insufficient exchangeable protons for CEST detection and for desirable treatment efficacy. To achieve sufficient CEST enhancement for imaging the drug distribution and release, certain biomaterial design could be applied to further enhance the drug concentration at target sites and thus the imaging and treatment efficacy, such as incorporating drugs in self-assembled peptide hydrogel or nanocomposite hydrogel.[129,131] CEST detectable drug pemetrexed was conjugated to a peptide to form an amphiphilic prodrug that could form self-assembly

https://doi.org/10.1021/acsnano.4c05923
ACS Nano 2024, 18, 33775−33791

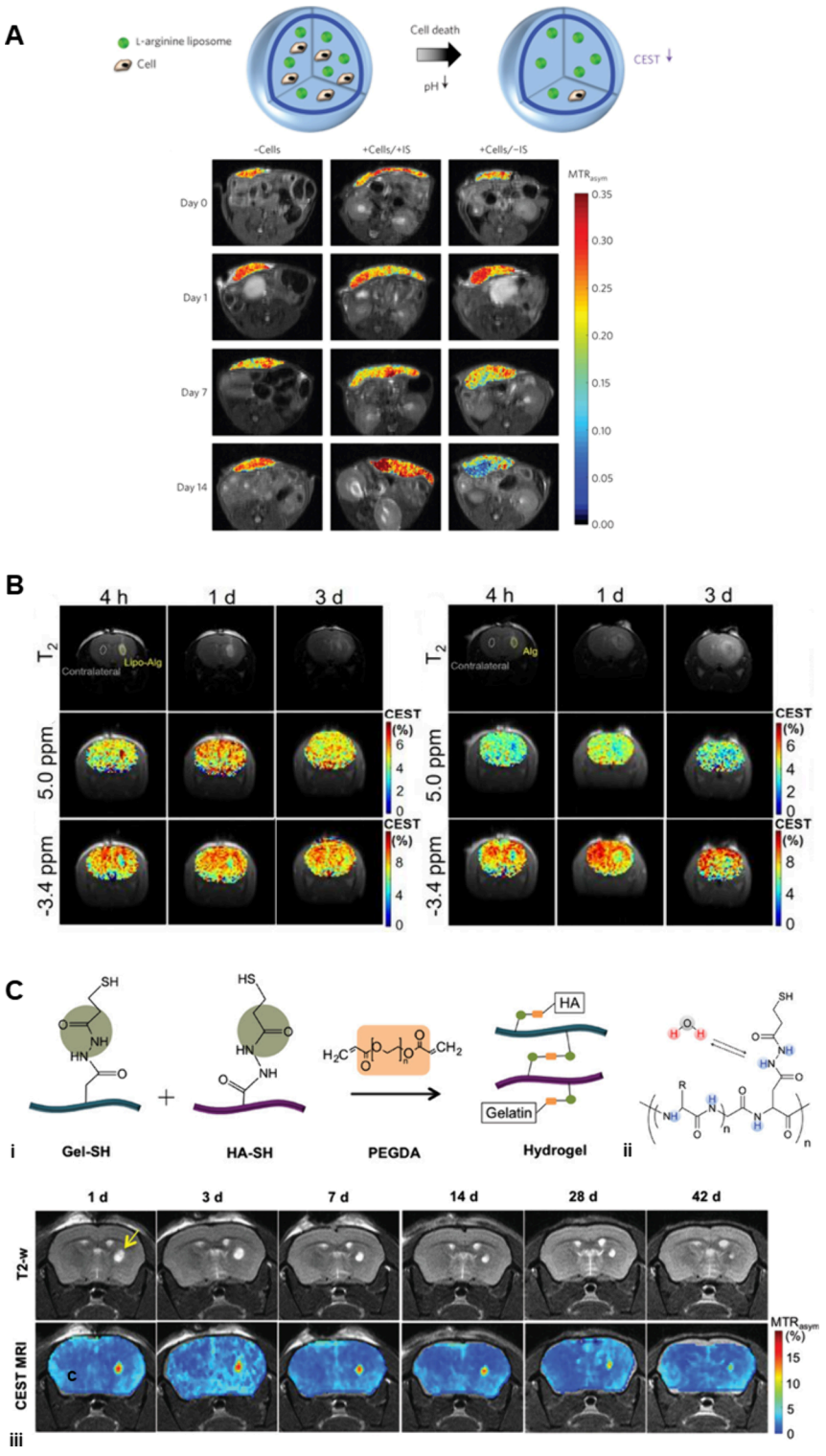

Figure 6. Nanocomposite Hydrogel-Based CEST CAs. (A) Within alginate hydrogel microcapsules that encapsulated L-arginine liposomes and hepatocytes, cell death could be detected by the reduced signal at 2 ppm of L-arginine liposomes, due to the decreased k_{ex} from the acidic environment. Reprinted from ref 68. Copyright 2013 The Authors. Published by Springer Nature. (B) Longitudinal monitoring of liposomal barbituric acid cargo embedded within alginate hydrogel (left panel; Lipo-Alg indicates site of injection) and control alginate hydrogel (right panel). Lipo-Alg nanocomposite hydrogel demonstrated two contrasts, 5 ppm for barbituric acid and −3.4 ppm for the liposome bilayer that can be monitored simultaneously. Reprinted under CC-BY License from ref 126. Copyright 2020 The Authors. Published by Ivyspring International Publisher. (C) i: Synthesis of PEGDA cross-linked gelatin/HA composite hydrogel, where the ratio of components would determine the stiffness and concentration of exchangeable protons. ii: Structure of thiolated gelatin having amide groups that exchange with water. iii: Label-free *in vivo* monitoring of Gel/HA/PEGDA composite hydrogel degradation. Reprinted with permission from ref 127. Copyright 2019 John Wiley and Sons.

https://doi.org/10.1021/acsnano.4c05923
ACS Nano 2024, 18, 33775−33791

Table 1. A List of Studies That Developed Nonparamagnetic CEST CAs for Detecting Molecular Events *in vivo*

Disease/Physiological process	Location	Molecular events assessed with CEST CA	CEST CA employed	CEST contrast offset (ppm)
Tumor	Brain	Agent delivery and distribution,[129,130] recovery process of hydrogel[129]	Injectable hydrogel formed by Pemetrexed-peptide conjugate,[129] maltitol[130]	5.2,[129] 1[130]
		Tumor hemodynamics[98]	Dextran of 1 kDa	∼1.2
		Distribution of liposome and encapsulated drug,[126,131] response to chemotherapeutic treatment[131]	Nanocomposite hydrogel with liposomal barbituric acid[126] and with liposomal gemcitabine and methotrexate coloaded[131]	5 and −3.4,[126] 2.4 and −3.5[131]
		Detection of transplanted tumor cells labeled with carbon dot liposome[74]	Liposome encapsulating carbon dots	2
	Subcutaneous xenograft	(glioblastoma) pHe change responding to treatment[132]	Iopamidol-liposome embedded alginate microbeads	4.2 (iopamidol), −3.4 (liposome)
		(lung cancer) Agent distribution and temporal evolution[133]	Tetraphenylporphine sulfonate ($TPPS_4$)	−9.75
		(melanoma) Temporal kinetics of glucose derivatives[134]	D-glucose and 3-O-methyl-D-glucose	1.2
		(leukemic cancer) Intracellular deoxycytidine kinase activity[89]	Deoxycytidine and its phosphorylated form	2
		Membrane antigen targeting in pancreatic and prostate cancer[121,135,136]	Dextran (10 kDa) with targeting moieties,[121,135] salicylic acid and antigen grafted polymeric agent[136]	1,[121,135] 7.2−11.8[136]
		(breast cancer) Increased vascular volume and acidic EES,[97] perfusion,[103] pH,[137,144] distinct agent distributions[138,142]	D-glucose,[97] four iodinated CT agents,[103] peptide hydrogel loaded with iopamidol,[137] salicylic acid based monomer agent/polymer agent/iopamidol,[144] dextran (70 kDa) and voluven (130 kDa),[138] PEG−PAM-PAN@DOX,[142]	0.8−2.2,[97] 4.3,[103] 4.2 and 5.5,[137] 5.0 and 9.2 for salicylic acid based agent and 4.2 and 5.6 for iopamidol,[144] ∼1,[138] ∼0.5,[142]
		(colon cancer) Longitudinal monitoring of agent distribution and response to TNF-α therapy,[119,139] vascular permeability,[106,118] tumor associated enzyme furin,[140] activity and inhibition of enzyme kallikrein 6 (KLK6)[86]	Liposome loaded with barbituric acid,[119] iodixanol liposome,[139] dextran of 10 kDa and 70 kDa[106] and 150 kDa,[118] olsalazine-peptide conjugate with furin-mediated intracellular reduction capability,[140] salicylic acid with a substrate for KLK6[86]	5,[119] 4.3,[139] 0.9,[106] 1,[118] 9.8,[140] 5.3 and 9.5[86]
	Liver	pH mapping in patients[141] and rodent orthotopic tumor model[145]	Ioversol	4.3
	Breast	Drug accumulation,[143] pHe[145]	Aspirin,[143] ioversol[145]	9.6,[143] 4.3[145]
	Ovary	γ-glutamyl transferase activity[85]	Salicylic acid with glutamyl ligand	4.8 and 9.2
Ischemic stroke	Brain	Drug distribution and targeted delivery[122]	Citicoline liposome	2
		Distribution, pH, temperature change[146]	Animal-derived extracellular matrix hydrogel	1.8 and 3.6
Alzheimer's Disease	Brain	Amyloid-β detection[147]	Angiopep-2	3.2
Acute kidney injury	Kidney	pH evolution[101]	Iopamidol	4.2 and 5.5
Physiological process	Lymph nodes	Lymphatic uptake[148]	Glycogen liposome, L-arginine liposome, and poly-L-lysine liposome	∼0.8 (glycogen liposome), ∼1.8−2.2 (L-arginine liposome), ∼3.6 (poly-L-lysine liposome)
	Subcutaneously transplanted xenogeneic hepatocytes	Fate of transplanted cells[68]	Alginate microspheres encapsulating L-arginine liposome and transplanted cells	2
	Brain	nose-to-brain drug delivery and distribution[123]	Mucus-penetrating liposome encapsulating iohexol	4.3 (iohexol), −3.4 (liposome), 1.2 (PEG)
		Binding of caffeine to less mobile substrate[113]	Caffeine	−1.5
	Kidney	pH mapping in mouse[100] and healthy volunteers[104]	Iopamidol	∼4.2 and 5.5
	Placenta	Glucose mapping in human placenta[149]	Glucose	0.75−4

https://doi.org/10.1021/acsnano.4c05923
ACS Nano 2024, 18, 33775−33791

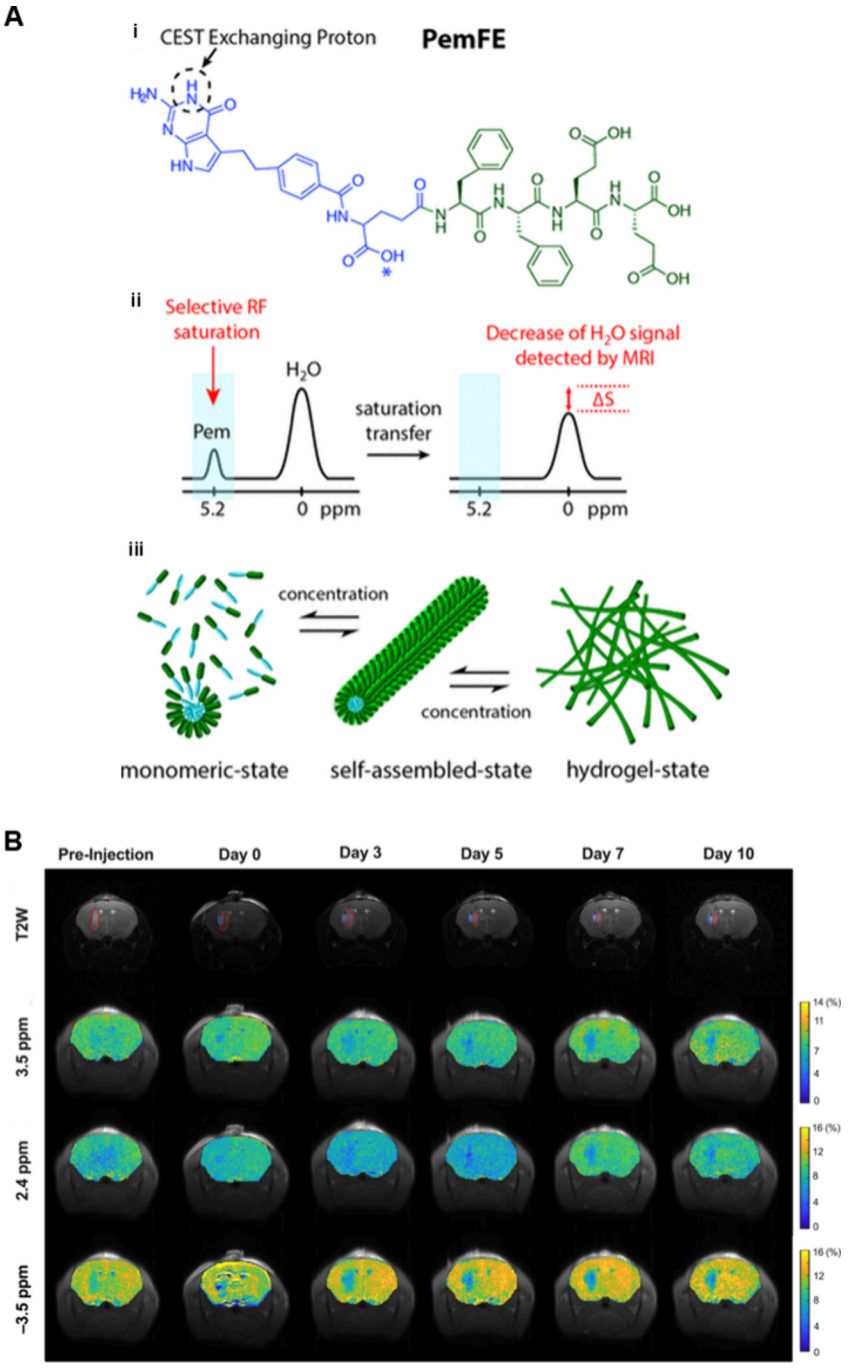

Figure 7. Approved therapeutic agents as theranostic CEST CAs. (A) i: pemetrexed-peptide (PemFE) conjugate was constructed with a designed peptide that facilitates amphiphilic balance and self-assembly. ii: Pem shows a CEST signal at 5.2 ppm. iii: PemFE monomer could undergo self-assembly and form filamentous nanostructures, which can further entangle into self-supporting hydrogels under suitable conditions. Reprinted with permission from ref 129. Copyright 2017 American Chemical Society. (B) Clinically used therapeutics gemcitabine and methotrexate incorporated into the liposomal hydrogel for local delivery to glioblastoma. Red line delineates tumor region and blue line for hydrogel region. Gemcitabine (2.4 ppm), liposome (−3.5 ppm in hydrogel region) and tumor treatment response (APT at 3.5 ppm, rNOE at −3.5 ppm) were monitored with CEST at their respective offset frequencies. Reprinted under CC-BY License from ref 131. Copyright 2024 The Authors. Published by MDPI.

through $\pi-\pi$ interactions and further into self-supporting hydrogels for longitudinal monitoring *in vivo* (Figure 7A).[129] By utilizing a tailor-made nanocarrier design of a nanocomposite hydrogel coloaded with gemcitabine liposome and methotrexate, CEST enables the multiparametric detection of the drugs as well as the tumor response to therapy longitudinally at 3T MRI.[131] With optimized liposome composition and hydrogel properties, imaging the liposomal drug release (at 2.4 ppm and −3.5 ppm, respectively, Figure 7B) from the hydrogel matrix is also feasible.[131]

There are numerous materials that could be used to enhance the sensitivity and specificity for detecting interesting biological events *in vivo*, such as liposomes, polymeric nanoparticles, nanocomposite hydrogel, and solvent systems. The

https://doi.org/10.1021/acsnano.4c05923
ACS Nano 2024, 18, 33775−33791

Scheme 2. CEST CAs Arranged by Desired Target Site (and Related Delivery Barrier Size) and Local Concentration[a]

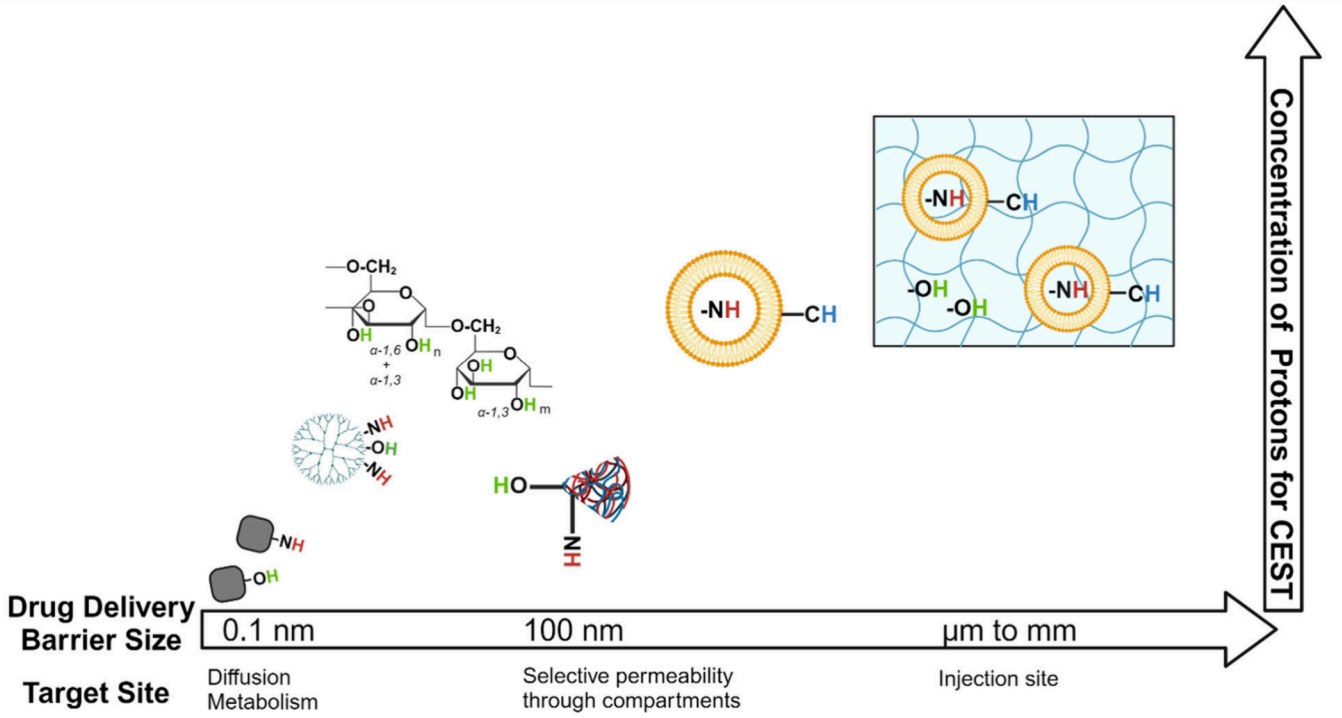

[a]CEST CAs at each position exhibit distinctive physicochemical and CEST properties that made them promising candidates for various biomedical applications. (Created with BioRender.com).

combination of CEST MRI with nanomedicine offers the opportunity for multicomponent imaging of the drug-nanocarrier system, facilitating the assessment of the endogenous exchange environment and optimization of delivery strategies simultaneously.

3.3. Tailor-Making Your CEST CA. Selection and design of CEST CAs should be informed by the physiologically or pathologically specific factors that determine the distribution and time window of the CEST contrast. Main determinants include the size, charge, and properties of the biological barrier (structurally and functionally) and molecular processes that alter the proton exchange (chemically). Taking the hydrophilic CT agent as an example, small-molecule CT agent solution could be directly administered to observe the pH-dependent CEST effect.[100] The biodistribution of CT agent is mainly diffusion-limited, as they can pass through the glomerular basement membrane with a pore size of 2−8 nm in the kidney.[152] Therefore, pH mapping with CEST in kidney, and evaluation of perfusion can be achieved.[100,103] However, the CEST signal of the CA (intravenously injected) could be quickly attenuated due to its short half-life of about 3−10 min in vascular and the interstitial spaces.[153]

To achieve longer circulation and higher local concentration for a broader time window for detection, liposome encapsulation of the CT agent is employed. With tailored liposome nanocarrier design, enhanced contrast for longer period of time is warranted, while simultaneously allowing label-free imaging of mucus layer penetration (iohexol-encapsulated liposome, size of 166 nm),[123] and heterogeneous and leaky tumor vasculature (iodixanol-encapsulated liposome, size of 165 nm).[139] Additionally, Kombala et al.[144] synthesized salicylic acid based monomer and polymer CEST CAs for pH detection. The polymer agent had >100 exchangeable protons and could be used at a concentration 488-fold lower than CT agent iopamidol. The nanocarrier approach employed in the above examples aligns with the design principle of increasing the local concentration of exchangeable protons in Section 2.1.

Scaling up further, 223 mM of iopamidol was incorporated into a peptide-based hydrogel matrix and showed discernible contrast for 9 h in a breast tumor mouse model.[137] Meanwhile, in another work where 972 mM iopamidol was encapsulated into liposome and then incorporated into alginate microbeads, 20 days of tumor pHe monitoring in response to bicarbonate treatment was demonstrated.[132] Overall, the three levels of size and complexity for CT agent based CEST CAs could serve the common purpose of contrast enhancement, and yet many different functions characteristic of each type of CA can be achieved: perfusion mapping for small-molecule CAs, selective permeation for nanocarrier form CAs, and prolonged local monitoring for nanocomposite hydrogel CA systems, echoing with the concepts illustrated in this review (Scheme 2).

Another series of studies highlighting the importance of CA design includes D-glucose and dextran. In a subcutaneous tumor model, D-glucose was rapidly metabolized in about 30 min, while for dextran of 10 kDa and dextran of 70 kDa, the retention of high MW dextran was observed.[97,106] This demonstrates that small molecules and their nanocarrier forms with properly selected sizes (dextran could range from 5.9 to 77 nm) could be used to probe tumor vasculature leakiness. Similar design rationale can also be found for liposome-based CEST CAs, where lymphatic drainage and intranasal mucus penetration were imaged with CEST liposomes around 100−150 nm.[123,148]

Toward the development of responsive theranostic CEST CAs, the "activation and retention" principle, or "pro-drug approach", could be applied, where a nontargeted CA can be

https://doi.org/10.1021/acsnano.4c05923
ACS Nano 2024, 18, 33775−33791

biochemically activated (enzymatically, for example) to accumulate at a target site.[154,155] Yuan et al.[140] has designed a smart molecule based on an anticancer drug, i.e., olsalazine with CEST contrast at 9.8 ppm. This molecule self-assembled into intracellular nanoparticles. In cancer cells with high furin expression, the cell-penetrating peptide would be cleaved, and then olsalazine nanoparticles could be retained. This smart theranostic approach, based on the "activation and retention" principle, provided a high intracellular concentration for CEST detection and was favorable for reducing off-target effect. This example demonstrates that we could make use of disease-specific biochemical environments to preserve or even enhance the CEST CA efficiency.

4. PROMISES AND CHALLENGES

Exogenous CEST CAs demonstrated success in detecting many molecular events *in vivo*. CEST is inherently sensitive to the exchange environment, and thus, further considerations are required when interpreting the changes in CEST contrast *in vivo*, which could be quite different from *in vitro* phantoms. Varying in size and properties, nonmetallic CEST CAs offer a wide range of tailor-made nanomedicine therapies with label-free image guidance. In Table 1, many successful studies showed that thoughtfully built CEST CAs with nanomaterial designs considering the *in vivo* biochemical aspects are promising. It is foreseeable that more biological processes could be imaged and assessed by CEST MRI. Such targeted and precise reporting on molecular information will greatly assist disease diagnosis and treatment planning.

The design of efficient CEST CAs is essential to detect many interesting molecular events *in vivo*, especially leveraging the advantages of CEST MRI such as label-free detection and high pH sensitivity as well as the recent advanced development in nanocarriers. Ideally, CEST CAs with a high number of exchangeable protons that are further away from the water signal, i.e., not overlapping with endogenous contrast at ±4 ppm, are desirable. For example, many therapeutics approved for clinical use, including drugs and biomaterials, could be repurposed to CEST CAs without additional metallic labels to enable the imaging of multiple components of administered therapeutics in various nanocarrier systems. A collection of anticancer drugs has been identified as CEST CAs.[46] Other therapeutics such as nonsteroidal anti-inflammatory drugs (NSAIDs), neuroprotective drugs, and cardiovascular drugs are waiting to be explored.

The advanced development in nanocarriers[156−158] could essentially help to preserve the CEST contrast *in vivo*, and to ensure a relatively high local concentration. As illustrated in Scheme 2, depending on the desired biodistribution and the molecular events, nanocarriers or nanocarrier-embedded composites can be constructed to load the small-molecule CEST CAs. A series of CEST CAs with nanocarrier components have been developed, such as liposomes, dendrimers, drug conjugates, and nanocomposite hydrogels (Table 1). Other nanostructures could potentially be applied as CEST nanocarriers, provided that they are endowed with proper water accessibility, which is a key factor for efficient CEST contrast (Scheme 1B). For example, modulation of water accessibility through liposome size, shape and bilayer composition could influence the water transport across the liposome and thus affect the resulting CEST contrast to different extents.[35,42,69] In contrast, poly(lactic-*co*-glycolic acid) (PLGA) has been commonly used as a drug carrier for chemotherapeutics with limited solubility in aqueous solution. Due to inadequate water accessibility, drugs in PLGA might not be able to generate CEST contrast. In this respect, nanocarriers such as extracellular vesicles, carbon-based nanomaterials, and metal−organic-framework (MOF) are potential candidates for constructing efficient and responsive CEST CAs.[74,112,159,160]

Extracellular vesicles (EVs) are a series of cell-secreted membrane carriers that vary in size (~30 nm to 5 μm) and biogenesis from parental cells.[159] Recently, mounting evidence suggests that EVs can be employed as an alternative for cell therapy and promising nanocarriers for a wide range of cargos for imaging.[161] Comparing with other lipidic nanocarriers, such as liposomes, EVs have the advantage of natural origin for a long circulation and cell-targeting capability, optimal size for passing various biological barriers including blood-brain barrier, and lysosomal evasion.[159] Multiple therapeutics and imaging agents can be loaded to EVs, achieving the theranostic function.[162] It is envisioned that with efficient extraction and cargo-loading techniques EVs would become efficient molecular CAs for label-free tracking of biological processes.

In summary, CEST is a nonrelaxation based MR imaging approach that detects many endogenous and exogenous molecules in a label-free manner. Thus, it enables the imaging of drugs, nanocarriers, and nanocomposite hydrogels *in vivo*. Importantly, it detects essential events for protons, providing valuable molecular information for assessing the drug delivery and molecular alterations upon treatments. Therefore, CEST is an indispensable approach for theranostic applications, with many successes having been shown in cancer. With rapidly emerging clinical CEST approaches and advanced nanotechnology, the application of CEST is envisioned to extend beyond cancer, encompassing various theranostic applications including neurodegenerative diseases.

AUTHOR INFORMATION

Corresponding Author

Kannie W. Y. Chan − *Department of Biomedical Engineering and Tung Biomedical Sciences Centre, City University of Hong Kong, Hong Kong, China; Hong Kong Centre for Cerebro-Cardiovascular Health Engineering (COCHE), Hong Kong, China; Russell H. Morgan Department of Radiology and Radiological Science, The Johns Hopkins University School of Medicine, Baltimore, Maryland 21287, United States; City University of Hong Kong Shenzhen Research Institute, Shenzhen 518057, China;* orcid.org/0000-0002-7315-1550; Email: KannieW.Y.C@cityu.edu.hk

Author

Haoyun Su − *Department of Biomedical Engineering, City University of Hong Kong, Hong Kong, China; Hong Kong Centre for Cerebro-Cardiovascular Health Engineering (COCHE), Hong Kong, China*

Complete contact information is available at: https://pubs.acs.org/10.1021/acsnano.4c05923

Notes

The authors declare no competing financial interest.

ACKNOWLEDGMENTS

This work was supported by Research Grants Council (11102218, 11200422, RFS2223-1S02, C1134-20G), City

https://doi.org/10.1021/acsnano.4c05923
ACS Nano 2024, 18, 33775−33791

University of Hong Kong (7005433, 7005626, 7030012, 9609321 and 9610616), HMRF (21222621), Tung Biomedical Sciences Centre, State Key Laboratory of Terahertz and Millimeter Waves and InnoHK Hong Kong Centre for Cerebro-cardiovascular Health Engineering. The Graphical Table of Content was created with Biorender.com.

VOCABULARY

Chemical exchange saturation transfer (CEST), an MRI approach that utilizes the continuous magnetization transfer between solute protons and bulk water protons to generate contrast in the form of a frequency-dependent reduction on water signal; Chemical exchange saturation transfer contrast agent (CEST CA), a compound that is administered to subjects to enhance contrast for CEST MRI. Paramagnetic agents, such as lanthanide complexes, hyperpolarized ^{129}Xe, and diamagnetic compounds are common CEST CAs; Theranostics, the concept where diagnosis and therapy are simultaneously implemented, usually with the aid of contrast materials; Nanomedicine, the use of nanometer sized materials for medicinal purposes; Label-free, in the context of CEST CAs, it refers to a type of CA where no additional fluorescent moieties, radioactive or metallic agents are incorporated into the CA only for the sake of generating contrast

REFERENCES

(1) Shuvaev, S.; Akam, E.; Caravan, P. Molecular MR Contrast Agents. *Invest. Radiol.* **2021**, *56*, 20−34.
(2) Mathur, M.; Jones, J. R.; Weinreb, J. C. Gadolinium Deposition and Nephrogenic Systemic Fibrosis: A Radiologist's Primer. *Radiographics* **2020**, *40*, 153−162.
(3) Zhou, J.; Payen, J. F.; Wilson, D. A.; Traystman, R. J.; van Zijl, P. C. M. Using the Amide Proton Signals of Intracellular Proteins and Peptides to Detect pH Effects in MRI. *Nat. Med.* **2003**, *9*, 1085−1090.
(4) Zhou, J.; Lal, B.; Wilson, D. A.; Laterra, J.; van Zijl, P. C. M. Amide Proton Transfer (APT) Contrast for Imaging of Brain Tumors. *Magn. Reson. Med.* **2003**, *50*, 1120−1126.
(5) Zhou, J.; Zaiss, M.; Knutsson, L.; Sun, P. Z.; Ahn, S. S.; Aime, S.; Bachert, P.; Blakeley, J. O.; Cai, K.; Chappell, M. A.; Chen, M.; Gochberg, D. F.; Goerke, S.; Heo, H. Y.; Jiang, S.; Jin, T.; Kim, S. G.; Laterra, J.; Paech, D.; Pagel, M. D.; et al. Review and Consensus Recommendations on Clinical APT-Weighted Imaging Approaches at 3T: Application to Brain Tumors. *Magn. Reson. Med.* **2022**, *88*, 546−574.
(6) Huang, J.; Chen, Z.; Park, S. W.; Lai, J. H. C.; Chan, K. W. Y. Molecular Imaging of Brain Tumors and Drug Delivery Using CEST MRI: Promises and Challenges. *Pharmaceutics* **2022**, *14*, 451.
(7) Wu, Y.; Sun, P. Z. Demonstration of pH Imaging in Acute Stroke with Endogenous Ratiometric Chemical Exchange Saturation Transfer Magnetic Resonance Imaging at 2 ppm. *NMR Biomed.* **2023**, *36*, No. e4850.
(8) Heo, H. Y.; Zhang, Y.; Burton, T. M.; Jiang, S.; Zhao, Y.; van Zijl, P. C. M.; Leigh, R.; Zhou, J. Improving the Detection Sensitivity of pH-Weighted Amide Proton Transfer MRI in Acute Stroke Patients Using Extrapolated Semisolid Magnetization Transfer Reference Signals. *Magn. Reson. Med.* **2017**, *78*, 871−880.
(9) Lai, J. H. C.; Liu, J.; Yang, T.; Huang, J.; Liu, Y.; Chen, Z.; Lee, Y.; Leung, G. K. K.; Chan, K. W. Y. Chemical Exchange Saturation Transfer Magnetic Resonance Imaging for Longitudinal Assessment of Intracerebral Hemorrhage and Deferoxamine Treatment at 3T in a Mouse Model. *Stroke* **2023**, *54*, 255−264.
(10) Li, Y.; Chen, H.; Xu, J.; Yadav, N. N.; Chan, K. W. Y.; Luo, L.; McMahon, M. T.; Vogelstein, B.; van Zijl, P. C. M.; Zhou, S.; Liu, G. CEST Theranostics: Label-Free MR Imaging of Anticancer Drugs. *Oncotarget* **2016**, *7*, 6369−6378.
(11) Mayne, L.; Paterson, Y.; Cerasoli, D.; Englander, S. W. Effect of Antibody Binding on Protein motions Studied by Hydrogen-Exchange Labeling and Two-Dimensional NMR. *Biochemistry* **1992**, *31*, 10678−10685.
(12) Lauzon, C. B.; van Zijl, P.; Stivers, J. T. Using the Water Signal to Detect Invisible Exchanging Protons in the Catalytic Triad of a Serine Protease. *J. Biomol. NMR* **2011**, *50*, 299−314.
(13) Roder, H.; Elove, G. A.; Englander, S. W. Structural Characterization of Folding Intermediates in Cytochrome C by H-Exchange Labelling and Proton NMR. *Nature* **1988**, *335*, 700−704.
(14) Mori, S.; Johnson, M. O.; Berg, J. M.; van Zijl, P. C. M. Water Exchange Filter (WEX Filter) for Nuclear-Magnetic-Resonance Studies of Macromolecules. *J. Am. Chem. Soc.* **1994**, *116*, 11982−11984.
(15) Ward, K. M.; Aletras, A. H.; Balaban, R. S. A New Class of Contrast Agents for MRI Based on Proton Chemical Exchange Dependent Saturation Transfer (CEST). *J. Magn. Reson.* **2000**, *143*, 79−87.
(16) van Zijl, P. C. M.; Lam, W. W.; Xu, J.; Knutsson, L.; Stanisz, G. J. Magnetization Transfer Contrast and Chemical Exchange Saturation Transfer MRI. Features and Analysis of the Field-Dependent Saturation Spectrum. *Neuroimage* **2018**, *168*, 222−241.
(17) Wolff, S. D.; Balaban, R. S. Magnetization Transfer Contrast (MTC) and Tissue Water Proton Relaxation In Vivo. *Magn. Reson. Med.* **1989**, *10*, 135−144.
(18) van Zijl, P. C. M.; Yadav, N. N. Chemical Exchange Saturation Transfer (CEST): What Is in a Name and What Isn't? *Magn. Reson. Med.* **2011**, *65*, 927−948.
(19) Togao, O.; Yoshiura, T.; Keupp, J.; Hiwatashi, A.; Yamashita, K.; Kikuchi, K.; Suzuki, Y.; Suzuki, S. O.; Iwaki, T.; Hata, N.; Mizoguchi, M.; Yoshimoto, K.; Sagiyama, K.; Takahashi, M.; Honda, H. Amide Proton Transfer Imaging of Adult Diffuse Gliomas: Correlation with Histopathological Grades. *Neuro Oncol.* **2014**, *16*, 441−448.
(20) Goldenberg, J. M.; Pagel, M. D. Assessments of Tumor Metabolism with CEST MRI. *NMR Biomed.* **2019**, *32*, No. e3943.
(21) Jiang, S.; Zou, T.; Eberhart, C. G.; Villalobos, M. A. V.; Heo, H. Y.; Zhang, Y.; Wang, Y.; Wang, X.; Yu, H.; Du, Y.; van Zijl, P. C. M.; Wen, Z.; Zhou, J. Predicting IDH Mutation Status in Grade II Gliomas Using Amide Proton Transfer-Weighted (APTw) MRI. *Magn. Reson. Med.* **2017**, *78*, 1100−1109.
(22) Ma, B.; Blakeley, J. O.; Hong, X.; Zhang, H.; Jiang, S.; Blair, L.; Zhang, Y.; Heo, H. Y.; Zhang, M.; van Zijl, P. C. M.; Zhou, J. Applying Amide Proton Transfer-Weighted MRI to Distinguish Pseudoprogression from True Progression in Malignant Gliomas. *J. Magn. Reson. Imaging* **2016**, *44*, 456−462.
(23) Cai, K.; Haris, M.; Singh, A.; Kogan, F.; Greenberg, J. H.; Hariharan, H.; Detre, J. A.; Reddy, R. Magnetic Resonance Imaging of Glutamate. *Nat. Med.* **2012**, *18*, 302−306.
(24) Cember, A. T. J.; Nanga, R. P. R.; Reddy, R. Glutamate-Weighted CEST (GluCEST) Imaging for Mapping Neurometabolism: An Update on the State of the Art and Emerging Findings from Applications. *NMR Biomed.* **2023**, *36*, No. e4780.
(25) Kogan, F.; Haris, M.; Debrosse, C.; Singh, A.; Nanga, R. P. R.; Cai, K.; Hariharan, H.; Reddy, R. In Vivo Chemical Exchange Saturation Transfer Imaging of Creatine (CrCEST) in Skeletal Muscle at 3T. *J. Magn. Reson. Imaging* **2014**, *40*, 596−602.
(26) Wang, K.; Huang, J.; Ju, L.; Xu, S.; Gullapalli, R. P.; Liang, Y.; Rogers, J.; Li, Y.; van Zijl, P. C. M.; Weiss, R. G.; Chan, K. W. Y.; Xu, J. Creatine Mapping of the Brain at 3T by CEST MRI. *Magn. Reson. Med.* **2024**, *91*, 51−60.
(27) Haris, M.; Nanga, R. P. R.; Singh, A.; Cai, K.; Kogan, F.; Hariharan, H.; Reddy, R. Exchange Rates of Creatine Kinase Metabolites: Feasibility of Imaging Creatine by Chemical Exchange Saturation Transfer MRI. *NMR Biomed.* **2012**, *25*, 1305−1309.
(28) Ju, L.; Wang, K.; Schär, M.; Xu, S.; Rogers, J.; Zhu, D.; Qin, Q.; Weiss, R. G.; Xu, J. Simultaneous Creatine and Phosphocreatine Mapping of Skeletal Muscle by CEST MRI at 3T. *Magn. Reson. Med.* **2024**, *91*, 942−954.

https://doi.org/10.1021/acsnano.4c05923
ACS Nano 2024, 18, 33775−33791

(29) Zhang, Z.; Wang, K.; Park, S.; Li, A.; Li, Y.; Weiss, R. G.; Xu, J. The Exchange Rate of Creatine CEST in Mouse Brain. *Magn. Reson. Med.* **2023**, *90*, 373−384.
(30) Haris, M.; Cai, K.; Singh, A.; Hariharan, H.; Reddy, R. In Vivo Mapping of Brain Myo-Inositol. *Neuroimage* **2011**, *54*, 2079−2085.
(31) Vinogradov, E.; Keupp, J.; Dimitrov, I. E.; Seiler, S.; Pedrosa, I. CEST-MRI For Body Oncologic Imaging: Are We There Yet? *NMR Biomed.* **2023**, *36*, No. e4906.
(32) van Zijl, P. C. M.; Jones, C. K.; Ren, J.; Malloy, C. R.; Sherry, A. D. MRI Detection of Glycogen In Vivo by Using Chemical Exchange Saturation Transfer Imaging (glycoCEST). *Proc. Natl. Acad. Sci. U. S. A.* **2007**, *104*, 4359−4364.
(33) Krishnamoorthy, G.; Nanga, R. P. R.; Bagga, P.; Hariharan, H.; Reddy, R. High Quality Three-Dimensional GagCEST Imaging of In Vivo Human Knee Cartilage at 7 T. *Magn. Reson. Med.* **2017**, *77*, 1866−1873.
(34) Schleich, C.; Muller-Lutz, A.; Zimmermann, L.; Boos, J.; Schmitt, B.; Wittsack, H. J.; Antoch, G.; Miese, F. Biochemical Imaging of Cervical Intervertebral Discs with Glycosaminoglycan Chemical Exchange Saturation Transfer Magnetic Resonance Imaging: Feasibility and Initial Results. *Skeletal Radiol.* **2016**, *45*, 79−85.
(35) Zu, Z.; Lin, E. C.; Louie, E. A.; Xu, J.; Li, H.; Xie, J.; Lankford, C. L.; Chekmenev, E. Y.; Swanson, S. D.; Does, M. D.; Gore, J. C.; Gochberg, D. F. Relayed Nuclear Overhauser Enhancement Sensitivity to Membrane Cho Phospholipids. *Magn. Reson. Med.* **2020**, *84*, 1961−1976.
(36) Chang, Y. C.; Liu, H. Q.; Chang, J. H.; Chang, Y. Y.; Lin, E. C. Role of the Cholesterol Hydroxyl Group in the Chemical Exchange Saturation Transfer Signal at −1.6 ppm. *NMR Biomed.* **2020**, *33*, No. e4356.
(37) Zhang, Y.; Zu, T.; Liu, R.; Zhou, J. Acquisition Sequences and Reconstruction Methods for Fast Chemical Exchange Saturation Transfer Imaging. *NMR Biomed.* **2023**, *36*, No. e4699.
(38) Zaiss, M.; Bachert, P. Chemical Exchange Saturation Transfer (CEST) and MR Z-Spectroscopy: A Review of Theoretical Approaches and Methods. *Phys. Med. Biol.* **2013**, *58*, R221−R269.
(39) Zhou, J.; Wilson, D. A.; Sun, P. Z.; Klaus, J. A.; Van Zijl, P. C. M. Quantitative Description of Proton Exchange Processes Between Water and Endogenous and Exogenous Agents for WEX, CEST, and APT Experiments. *Magn. Reson. Med.* **2004**, *51*, 945−952.
(40) Wu, Y.; Evbuomwan, M.; Melendez, M.; Opina, A.; Sherry, A. D. Advantages of Macromolecular to Nanosized Chemical-Exchange Saturation Transfer Agents for MRI Applications. *Future Med. Chem.* **2010**, *2*, 351−366.
(41) Chan, K. W. Y.; Bulte, J. W. M.; McMahon, M. T. Diamagnetic Chemical Exchange Saturation Transfer (DiaCEST) Liposomes: Physicochemical Properties and Imaging Applications. *Wiley Interdiscip. Rev.: Nanomed. Nanobiotechnol.* **2014**, *6*, 111−124.
(42) Ferrauto, G.; Castelli, D. D.; Di Gregorio, E.; Terreno, E.; Aime, S. LipoCEST and CellCEST Imaging Agents: Opportunities and Challenges. *Wiley Interdiscip. Rev.: Nanomed. Nanobiotechnol.* **2016**, *8*, 602−618.
(43) McMahon, M. T.; Bulte, J. W. M. Two Decades of Dendrimers As Versatile MRI Agents: A Tale With and Without Metals. *Wiley Interdiscip. Rev.: Nanomed. Nanobiotechnol.* **2018**, *10*, No. e1496.
(44) Han, Z.; Liu, G. Sugar-Based Biopolymers as Novel Imaging Agents for Molecular Magnetic Resonance Imaging. *Wiley Interdiscip. Rev.: Nanomed. Nanobiotechnol.* **2019**, *11*, No. e1551.
(45) Jia, Y.; Geng, K.; Cheng, Y.; Li, Y.; Chen, Y.; Wu, R. Nanomedicine Particles Associated with Chemical Exchange Saturation Transfer Contrast Agents in Biomedical Applications. *Front. Chem.* **2020**, *8*, 326.
(46) Chen, Z.; Han, Z.; Liu, G. Repurposing Clinical Agents for Chemical Exchange Saturation Transfer Magnetic Resonance Imaging: Current Status and Future Perspectives. *Pharmaceuticals* **2021**, *14*, 11.
(47) Han, Z.; Liu, G. CEST MRI Trackable Nanoparticle Drug Delivery Systems. *Biomed. Mater.* **2021**, *16*, 024103.
(48) Ferrauto, G.; Terreno, E. Compartmentalized Agents: A Powerful Strategy for Enhancing the Detection Sensitivity of Chemical Exchange Saturation Transfer Contrast. *NMR Biomed.* **2023**, *36*, No. e4791.
(49) Longo, D. L.; Carella, A.; Corrado, A.; Pirotta, E.; Mohanta, Z.; Singh, A.; Stabinska, J.; Liu, G.; McMahon, M. T. A Snapshot of the Vast Array of Diamagnetic CEST MRI Contrast Agents. *NMR Biomed.* **2023**, *36*, No. e4715.
(50) Liu, G.; Song, X.; Chan, K. W. Y.; McMahon, M. T. Nuts and Bolts of Chemical Exchange Saturation Transfer MRI. *NMR Biomed.* **2013**, *26*, 810−828.
(51) Bie, C.; van Zijl, P.; Xu, J.; Song, X.; Yadav, N. N. Radiofrequency Labeling Strategies in Chemical Exchange Saturation Transfer MRI. *NMR Biomed.* **2023**, *36*, No. e4944.
(52) Zaiss, M.; Jin, T.; Kim, S. G.; Gochberg, D. F. Theory of Chemical Exchange Saturation Transfer MRI in the Context of Different Magnetic Fields. *NMR Biomed.* **2023**, *36*, No. e4961.
(53) Alsop, D. C.; Ercan, E.; Girard, O. M.; Mackay, A. L.; Michal, C. A.; Varma, G.; Vinogradov, E.; Duhamel, G. Inhomogeneous Magnetization Transfer Imaging: Concepts and Directions for Further Development. *NMR Biomed.* **2023**, *36*, No. e4808.
(54) Sherry, A. D.; Castelli, D. D.; Aime, S. Prospects and Limitations of Paramagnetic Chemical Exchange Saturation Transfer Agents Serving As Biological Reporters In Vivo. *NMR Biomed.* **2023**, *36*, No. e4698.
(55) Xu, J.; Chung, J. J.; Jin, T. Chemical Exchange Saturation Transfer Imaging of Creatine, Phosphocreatine, and Protein Arginine Residue in Tissues. *NMR Biomed.* **2023**, *36*, No. e4671.
(56) Zhou, Y.; Bie, C.; van Zijl, P. C. M.; Yadav, N. N. The Relayed Nuclear Overhauser Effect in Magnetization Transfer and Chemical Exchange Saturation Transfer MRI. *NMR Biomed.* **2023**, *36*, No. e4778.
(57) Gilad, A. A.; Bar-Shir, A.; Bricco, A. R.; Mohanta, Z.; McMahon, M. T. Protein and Peptide Engineering for Chemical Exchange Saturation Transfer Imaging in the Age of Synthetic Biology. *NMR Biomed.* **2023**, *36*, No. e4712.
(58) Cember, A. T. J.; Nanga, R. P. R.; Reddy, R. Glutamate-Weighted CEST (GluCEST) Imaging for Mapping Neurometabolism: An Update on the State of the Art and Emerging Findings From In Vivo Applications. *NMR Biomed.* **2023**, *36*, No. e4780.
(59) Jiang, S.; Wen, Z.; Ahn, S. S.; Cai, K.; Paech, D.; Eberhart, C. G.; Zhou, J. Applications of Chemical Exchange Saturation Transfer Magnetic Resonance Imaging in Identifying Genetic Markers in Gliomas. *NMR Biomed.* **2023**, *36*, No. e4731.
(60) Cho, N. S.; Hagiwara, A.; Yao, J.; Nathanson, D. A.; Prins, R. M.; Wang, C.; Raymond, C.; Desousa, B. R.; Divakaruni, A.; Morrow, D. H.; Nghiemphu, P. L.; Lai, A.; Liau, L. M.; Everson, R. G.; Salamon, N.; Pope, W. B.; Cloughesy, T. F.; Ellingson, B. M. Amine-Weighted Chemical Exchange Saturation Transfer Magnetic Resonance Imaging in Brain Tumors. *NMR Biomed.* **2023**, *36*, No. e4785.
(61) Igarashi, T.; Kim, H.; Sun, P. Z. Detection of Tissue pH With Quantitative Chemical Exchange Saturation Transfer Magnetic Resonance Imaging. *NMR Biomed.* **2023**, *36*, No. e4711.
(62) Heo, H. Y.; Tee, Y. K.; Harston, G.; Leigh, R.; Chappell, M. A. Amide Proton Transfer Imaging in Stroke. *NMR Biomed.* **2023**, *36*, No. e4734.
(63) Huang, J.; Lai, J. H. C.; Han, X.; Chen, Z.; Xiao, P.; Liu, Y.; Chen, L.; Xu, J.; Chan, K. W. Y. Sensitivity Schemes for Dynamic Glucose-Enhanced Magnetic Resonance Imaging to Detect Glucose Uptake and Clearance in Mouse Brain at 3 T. *NMR Biomed.* **2023**, *36*, No. e4962.
(64) Perlman, O.; Farrar, C. T.; Heo, H. Y. MR Fingerprinting for Semisolid Magnetization Transfer and Chemical Exchange Saturation Transfer Quantification. *NMR Biomed.* **2023**, *36*, No. e4710.
(65) Xu, J.; Chung, J. J.; Jin, T. Chemical Exchange Saturation Transfer Imaging of Creatine, Phosphocreatine, and Protein Arginine Residue in Tissues. *NMR Biomed.* **2023**, *36*, No. e4671.

https://doi.org/10.1021/acsnano.4c05923
ACS Nano 2024, 18, 33775−33791

(66) Jones, K. M.; Pollard, A. C.; Pagel, M. D. Clinical Applications of Chemical Exchange Saturation Transfer (CEST) MRI. *J. of Magn. Reson. Imaging* **2018**, *47*, 11−27.
(67) Jin, T.; Kim, S. G. Approximated Analytical Characterization of the Steady-State Chemical Exchange Saturation Transfer (CEST) Signals. *Magn. Reson. Med.* **2019**, *82*, 1876−1889.
(68) Chan, K. W. Y.; Liu, G.; Song, X.; Kim, H.; Yu, T.; Arifin, D. R.; Gilad, A. A.; Hanes, J.; Walczak, P.; van Zijl, P. C. M.; Bulte, J. W. M.; McMahon, M. T. MRI-Detectable pH Nanosensors Incorporated Into Hydrogels for Sensing of Transplanted-Cell Viability. *Nat. Mater.* **2013**, *12*, 268−275.
(69) Zhao, J. M.; Har-El, Y. E.; McMahon, M. T.; Zhou, J.; Sherry, A. D.; Sgouros, G.; Bulte, J. W. M.; van Zijl, P. C. M. Size-Induced Enhancement of Chemical Exchange Saturation Transfer (CEST) Contrast in Liposomes. *J. Am. Chem. Soc.* **2008**, *130*, 5178−5184.
(70) Demetriou, E.; Story, H. E.; Bofinger, R.; Hailes, H. C.; Tabor, A. B.; Golay, X. Effect of Liposomal Encapsulation on the Chemical Exchange Properties of Diamagnetic CEST Agents. *J. Phys. Chem. B* **2019**, *123*, 7545−7557.
(71) Ferrauto, G.; Aime, S.; McMahon, M. T.; Morrow, J. R.; Snyder, E. M.; Li, A.; Bartha, R. Chemical Exchange Saturation Transfer (CEST) Contrast Agents. In *Contrast Agents for MRI: Experimental Methods*; Pierre, V. C.; Allen, M. J., Eds.; The Royal Society of Chemistry, 2017; pp 243−317.
(72) Snoussi, K.; Bulte, J. W. M.; Gueron, M.; van Zijl, P. C. M. Sensitive CEST Agents Based on Nucleic Acid Imino Proton Exchange: Detection of Poly(rU) and of a Dendrimer-Poly(rU) Model for Nucleic Acid Delivery and Pharmacology. *Magn. Reson. Med.* **2003**, *49*, 998−1005.
(73) Lesniak, W. G.; Oskolkov, N.; Song, X.; Lal, B.; Yang, X.; Pomper, M.; Laterra, J.; Nimmagadda, S.; McMahon, M. T. Salicylic Acid Conjugated Dendrimers Are a Tunable, High Performance CEST MRI NanoPlatform. *Nano Lett.* **2016**, *16*, 2248−2253.
(74) Zhang, J.; Yuan, Y.; Gao, M.; Han, Z.; Chu, C.; Li, Y.; van Zijl, P. C. M.; Ying, M.; Bulte, J. W. M.; Liu, G. Carbon Dots as a New Class of Diamagnetic Chemical Exchange Saturation Transfer (diaCEST) MRI Contrast Agents. *Angew. Chem., Int. Ed.* **2019**, *58*, 9871−9875.
(75) Longo, D. L.; Moustaghfir, F. Z.; Zerbo, A.; Consolino, L.; Anemone, A.; Bracesco, M.; Aime, S. EXCI-CEST: Exploiting Pharmaceutical Excipients As MRI-CEST Contrast Agents for Tumor Imaging. *Int. J. Pharm.* **2017**, *525*, 275−281.
(76) Sadeghi-Oroumiyeh, A.; Valizadeh, H.; Zakeri-Milani, P. Determination of Paclitaxel Solubility and Stability in the Presence of Injectable Excipients. *Pharm. Chem. J.* **2021**, *55*, 983−987.
(77) Seedher, N.; Bhatia, S. Solubility Enhancement of Cox-2 Inhibitors Using Various Solvent Systems. *AAPS PharmSciTech* **2003**, *4*, No. 36.
(78) Simamora, P.; Alvarez, J. M.; Yalkowsky, S. H. Solubilization of Rapamycin. *Int. J. Pharm.* **2001**, *213*, 25−29.
(79) Su, H.; Law, L. H.; Liu, Y.; Huang, J.; Chan, K. W. Y. CEST Effect of Dimethyl Sulfoxide (DMSO) at Negative Offset Frequency. *NMR Biomed.* **2024**, DOI: 10.1002/nbm.5238, *In Press*.
(80) Bar-Shir, A.; Bulte, J. W. M.; Gilad, A. A. Molecular Engineering of Nonmetallic Biosensors for CEST MRI. *ACS Chem. Biol.* **2015**, *10*, 1160−1170.
(81) Haris, M.; Singh, A.; Mohammed, I.; Ittyerah, R.; Nath, K.; Nanga, R. P. R.; Debrosse, C.; Kogan, F.; Cai, K.; Poptani, H.; Reddy, D.; Hariharan, H.; Reddy, R. In Vivo Magnetic Resonance Imaging of Tumor Protease Activity. *Sci. Rep.* **2014**, *4*, 6081.
(82) Bar-Shir, A.; Liu, G.; Greenberg, M. M.; Bulte, J. W. M.; Gilad, A. A. Synthesis of a Probe for Monitoring HSV1-tk Reporter Gene Expression Using Chemical Exchange Saturation Transfer MRI. *Nat. Protoc.* **2013**, *8*, 2380−2391.
(83) Sinharay, S.; Fernández-Cuervo, G.; Acfalle, J. P.; Pagel, M. D. Detection of Sulfatase Enzyme Activity with a CatalyCEST MRI Contrast Agent. *Chem. - Eur. J.* **2016**, *22*, 6491−6495.
(84) Daryaei, I.; Mohammadebrahim Ghaffari, M.; Jones, K. M.; Pagel, M. D. Detection of Alkaline Phosphatase Enzyme Activity with a CatalyCEST MRI Biosensor. *ACS Sens.* **2016**, *1*, 857−861.
(85) Sinharay, S.; Randtke, E. A.; Jones, K. M.; Howison, C. M.; Chambers, S. K.; Kobayashi, H.; Pagel, M. D. Noninvasive Detection of Enzyme Activity in Tumor Models of Human Ovarian Cancer Using CatalyCEST MRI. *Magn. Reson. Med.* **2017**, *77*, 2005−2014.
(86) Sinharay, S.; Randtke, E. A.; Howison, C. M.; Ignatenko, N. A.; Pagel, M. D. Detection of Enzyme Activity and Inhibition during Studies in Solution, In Vitro and In Vivo with CatalyCEST MRI. *Mol. Imaging Biol.* **2018**, *20*, 240−248.
(87) Kombala, C. J.; Lokugama, S. D.; Kotrotsou, A.; Li, T.; Pollard, A. C.; Pagel, M. D. Simultaneous Evaluations of pH and Enzyme Activity with a CEST MRI Contrast Agent. *ACS Sens.* **2021**, *6*, 4535−4544.
(88) Liu, G.; Liang, Y.; Bar-Shir, A.; Chan, K. W. Y.; Galpoththawela, C. S.; Bernard, S. M.; Tse, T.; Yadav, N. N.; Walczak, P.; McMahon, M. T.; Bulte, J. W. M.; van Zijl, P. C. M.; Gilad, A. A. Monitoring Enzyme Activity Using a Diamagnetic Chemical Exchange Saturation Transfer Magnetic Resonance Imaging Contrast Agent. *J. Am. Chem. Soc.* **2011**, *133*, 16326−16329.
(89) Han, Z.; Li, Y.; Zhang, J.; Liu, J.; Chen, C.; van Zijl, P. C. M; Liu, G. Molecular Imaging of Deoxycytidine Kinase Activity Using Deoxycytidine-Enhanced CEST MRI. *Cancer Res.* **2019**, *79*, 2775−2783.
(90) Brun, E. M. S. P. T.; Calvert, N. D.; Suchy, M.; Kirby, A.; Melkus, G.; Garipov, R.; Addison, C. L.; Shuhendler, A. J. Mapping Vitamin B Metabolism by HydrazoCEST Magnetic Resonance Imaging. *Chem. Commun.* **2021**, *57*, 10867−10870.
(91) Yu, F. F.; Rathnakar, J.; Ryder, B.; Hitt, B.; Kashmer, O. M.; Sherry, A. D.; Vinogradov, E. Differentiation and Characterization of Healthy Versus Pathological Tau Using Chemical Exchange Saturation Transfer. *NMR Biomed.* **2024**, *37*, e5160.
(92) Goerke, S.; Zaiss, M.; Kunz, P.; Klika, K. D.; Windschuh, J. D.; Mogk, A.; Bukau, B.; Ladd, M. E.; Bachert, P. Signature of Protein Unfolding in Chemical Exchange Saturation Transfer Imaging. *NMR Biomed.* **2015**, *28*, 906−913.
(93) Goerke, S.; Milde, K. S.; Bukowiecki, R.; Kunz, P.; Klika, K. D.; Wiglenda, T.; Mogk, A.; Wanker, E. E.; Bukau, B.; Ladd, M. E.; Bachert, P.; Zaiss, M. Aggregation-Induced Changes in the Chemical Exchange Saturation Transfer (CEST) Signals of Proteins. *NMR Biomed.* **2017**, *30*, No. e3665.
(94) Brettschneider, J.; Tredici, K. D.; Lee, V. M.-Y.; Trojanowski, J. Q. Spreading of Pathology in Neurodegenerative Diseases: A Focus on Human Studies. *Nat. Rev. Neurosci.* **2015**, *16*, 109−120.
(95) Yang, X.; Yadav, N. N.; Song, X.; Ray Banerjee, S.; Edelman, H.; Minn, I.; van Zijl, P. C. M.; Pomper, M. G.; McMahon, M. T. Tuning Phenols with Intra-Molecular Bond Shifted HYdrogens (IMSHY) as DiaCEST MRI Contrast Agents. *Chemistry* **2014**, *20*, 15824−15832.
(96) Chakraborty, S.; Peruncheralathan, S.; Ghosh, A. Paracetamol and Other Acetanilide Analogs As Inter-Molecular Hydrogen Bonding Assisted Diamagnetic CEST MRI Contrast Agents. *RSC Adv.* **2021**, *11*, 6526−6534.
(97) Chan, K. W. Y.; McMahon, M. T.; Kato, Y.; Liu, G.; Bulte, J. W. M.; Bhujwalla, Z. M.; Artemov, D.; van Zijl, P. C. M. Natural D-glucose As a Biodegradable MRI Contrast Agent for Detecting Cancer. *Magn. Reson. Med.* **2012**, *68*, 1764−1773.
(98) Han, Z.; Chen, C.; Xu, X.; Bai, R.; Staedtke, V.; Huang, J.; Chan, K. W. Y.; Xu, J.; Kamson, D. O.; Wen, Z.; Knutsson, L.; van Zijl, P. C. M.; Liu, G. Dynamic Contrast-Enhanced CEST MRI Using a Low Molecular Weight Dextran. *NMR Biomed.* **2022**, *35*, No. e4649.
(99) Bar-Shir, A.; Liu, G.; Liang, Y.; Yadav, N. N.; McMahon, M. T.; Walczak, P.; Nimmagadda, S.; Pomper, M. G.; Tallman, K. A.; Greenberg, M. M.; van Zijl, P. C. M.; Bulte, J. W. M; Gilad, A. A. Transforming Thymidine Into a Magnetic Resonance Imaging Probe for Monitoring Gene Expression. *J. Am. Chem. Soc.* **2013**, *135*, 1617−1624.

(100) Longo, D. L.; Dastrù, W.; Digilio, G.; Keupp, J.; Langereis, S.; Lanzardo, S.; Prestigio, S.; Steinbach, O.; Terreno, E.; Uggeri, F.; Aime, S. Iopamidol As a Responsive MRI-Chemical Exchange Saturation Transfer Contrast Agent for pH Mapping of Kidneys: In Vivo Studies in Mice at 7 T. *Magn. Reson. Med.* **2011**, *65*, 202−211.
(101) Longo, D. L.; Busato, A.; Lanzardo, S.; Antico, F.; Aime, S. Imaging the pH Evolution of an Acute Kidney Injury Model by Means of Iopamidol, a MRI-CEST pH-Responsive Contrast Agent. *Magn. Reson. Med.* **2013**, *70*, 859−864.
(102) Longo, D. L.; Sun, P. Z.; Consolino, L.; Michelotti, F. C.; Uggeri, F.; Aime, S. A General MRI-CEST Ratiometric Approach for pH Imaging: Demonstration of In Vivo pH Mapping with Iobitridol. *J. Am. Chem. Soc.* **2014**, *136*, 14333−14336.
(103) Longo, D. L.; Michelotti, F.; Consolino, L.; Bardini, P.; Digilio, G.; Xiao, G.; Sun, P. Z.; Aime, S. In Vitro and In Vivo Assessment of Nonionic Iodinated Radiographic Molecules as Chemical Exchange Saturation Transfer Magnetic Resonance Imaging Tumor Perfusion Agents. *Invest. Radiol.* **2016**, *51*, 155−162.
(104) Müller-Lutz, A.; Khalil, N.; Schmitt, B.; Jellus, V.; Pentang, G.; Oeltzschner, G.; Antoch, G.; Lanzman, R. S.; Wittsack, H. J. Pilot Study of Iopamidol-Based Quantitative pH Imaging on a Clinical 3T MR Scanner. *Magn. Reson. Mater. Phys., Biol. Med.* **2014**, *27*, 477−485.
(105) Chen, L. Q.; Randtke, E. A.; Jones, K. M.; Moon, B. F.; Howison, C. M.; Pagel, M. D. Evaluations of Tumor Acidosis Within Tumor Models Using Parametric Maps Generated with AcidoCEST MRI. *Mol. Imaging Biol.* **2015**, *17*, 488−496.
(106) Li, Y.; Qiao, Y.; Chen, H.; Bai, R.; Staedtke, V.; Han, Z.; Xu, J.; Chan, K. W. Y.; Yadav, N. N.; Bulte, J. W. M.; Zhou, S.; van Zijl, P. C. M.; Liu, G. Characterization of Tumor Vascular Permeability Using Natural Dextrans and CEST MRI. *Magn. Reson. Med.* **2018**, *79*, 1001−1009.
(107) Zaiss, M.; Zu, Z.; Xu, J.; Schuenke, P.; Gochberg, D. F.; Gore, J. C.; Ladd, M. E.; Bachert, P. A Combined Analytical Solution for Chemical Exchange Saturation Transfer and Semi-Solid Magnetization Transfer. *NMR Biomed.* **2015**, *28*, 217−230.
(108) Zaiss, M.; Angelovski, G.; Demetriou, E.; McMahon, M. T.; Golay, X.; Scheffler, K. QUESP and QUEST Revisited - Fast and Accurate Quantitative CEST Experiments. *Magn. Reson. Med.* **2018**, *79*, 1708−1721.
(109) Scheidegger, R.; Vinogradov, E.; Alsop, D. C. Amide Proton Transfer Imaging with Improved Robustness to Magnetic Field Inhomogeneity and Magnetization Transfer Asymmetry Using Saturation with Frequency Alternating RF Irradiation. *Magn. Reson. Med.* **2011**, *66*, 1275−1285.
(110) Xu, J.; Yadav, N. N.; Bar-Shir, A.; Jones, C. K.; Chan, K. W. C.; Zhang, J.; Walczak, P.; McMahon, M. T.; van Zijl, P. C. M. Variable Delay Multi-Pulse Train for Fast Chemical Exchange Saturation Transfer and Relayed-Nuclear Overhauser Enhancement MRI. *Magn. Reson. Med.* **2014**, *71*, 1798−1812.
(111) Jin, T.; Autio, J.; Obata, T.; Kim, S. G. Spin-locking Versus Chemical Exchange Saturation Transfer MRI for Investigating Chemical Exchange Process Between Water and Labile Metabolite Protons. *Magn. Reson. Med.* **2011**, *65*, 1448−1460.
(112) Jayapaul, J.; Schroder, L. Nanoparticle-Based Contrast Agents for (129)Xe HyperCEST NMR and MRI Applications. *Contrast Media Mol. Imaging* **2019**, *2019*, 9498173.
(113) Yadav, N. N.; Yang, X.; Li, Y.; Li, W.; Liu, G.; van Zijl, P. C. M. Detection of Dynamic Substrate Binding Using MRI. *Sci. Rep.* **2017**, *7*, 10138.
(114) Zhou, Y.; Bie, C.; van Zijl, P. C. M.; Xu, J.; Zou, C.; Yadav, N. N. Detection of Electrostatic Molecular Binding Using the Water Proton Signal. *Magn. Reson. Med.* **2022**, *88*, 901−915.
(115) Bar-Shir, A.; Gilad, A. A.; Chan, K. W. C.; Liu, G.; van Zijl, P. C. M.; Bulte, J. W. M.; McMahon, M. T. Metal Ion Sensing Using Ion Chemical Exchange Saturation Transfer (19)F Magnetic Resonance Imaging. *J. Am. Chem. Soc.* **2013**, *135*, 12164−12167.
(116) Bar-Shir, A.; Yadav, N. N.; Gilad, A. A.; van Zijl, P. C. M.; McMahon, M. T.; Bulte, J. W. M. Single (19)F Probe for Simultaneous Detection of Multiple Metal Ions Using miCEST MRI. *J. Am. Chem. Soc.* **2015**, *137*, 78−81.
(117) Walker-Samuel, S.; Ramasawmy, R.; Torrealdea, F.; Rega, M.; Rajkumar, V.; Johnson, S. P.; Richardson, S.; Goncalves, M.; Parkes, H. G.; Arstad, E.; Thomas, D. L.; Pedley, R. B.; Lythgoe, M. F.; Golay, X. In Vivo Imaging of Glucose Uptake and Metabolism in Tumors. *Nat. Med.* **2013**, *19*, 1067−1072.
(118) Chen, H.; Liu, D.; Li, Y.; Xu, X.; Xu, J.; Yadav, N. N.; Zhou, S.; van Zijl, P. C. M.; Liu, G. CEST MRI Monitoring of Tumor Response to Vascular Disrupting Therapy Using High Molecular Weight Dextrans. *Magn. Reson. Med.* **2019**, *82*, 1471−1479.
(119) Chan, K. W. Y.; Yu, T.; Qiao, Y.; Liu, Q.; Yang, M.; Patel, H.; Liu, G.; Kinzler, K. W.; Vogelstein, B.; Bulte, J. W. M.; van Zijl, P. C. M.; Hanes, J.; Zhou, S.; McMahon, M. T. A DiaCEST MRI Approach for Monitoring Liposomal Accumulation in Tumors. *J. Controlled Release* **2014**, *180*, 51−59.
(120) Yang, X.; Song, X.; Li, Y.; Liu, G.; Ray Banerjee, S.; Pomper, M. G.; McMahon, M. T. Salicylic Acid and Analogues As DiaCEST MRI Contrast Agents with Highly Shifted Exchangeable Proton Frequencies. *Angew. Chem., Int. Ed. Engl.* **2013**, *52*, 8116−8119.
(121) Liu, G.; Banerjee, S. R.; Yang, X.; Yadav, N.; Lisok, A.; Jablonska, A.; Xu, J.; Li, Y.; Pomper, M. G.; van Zijl, P. C. M. A Dextran-Based Probe for the Targeted Magnetic Resonance Imaging of Tumours Expressing Prostate-Specific Membrane Antigen. *Nat. Biomed. Eng.* **2017**, *1*, 977−982.
(122) Liu, H.; Jablonska, A.; Li, Y.; Cao, S.; Liu, D.; Chen, H.; Van Zijl, P. C. M.; Bulte, J. W. M.; Janowski, M.; Walczak, P.; Liu, G. Label-Free CEST MRI Detection of Citicoline-Liposome Drug Delivery in Ischemic Stroke. *Theranostics* **2016**, *6*, 1588−1600.
(123) Law, L. H.; Huang, J.; Xiao, P.; Liu, Y.; Chen, Z.; Lai, J. H. C.; Han, X.; Cheng, G. W. Y.; Tse, K. H.; Chan, K. W. Y. Multiple CEST Contrast Imaging of Nose-To-Brain Drug Delivery Using Iohexol Liposomes at 3T MRI. *J. Controlled Release* **2023**, *354*, 208−220.
(124) Merino, S.; Martin, C.; Kostarelos, K.; Prato, M.; Vazquez, E. Nanocomposite Hydrogels: 3D Polymer-Nanoparticle Synergies for On-Demand Drug Delivery. *ACS Nano* **2015**, *9*, 4686−97.
(125) Zhu, H.; Zheng, J.; Oh, X. Y.; Chan, C. Y.; Low, B. Q. L.; Tor, J. Q.; Jiang, W.; Ye, E.; Loh, X. J.; Li, Z. Nanoarchitecture-Integrated Hydrogel Systems toward Therapeutic Applications. *ACS Nano* **2023**, *17*, 7953−7978.
(126) Han, X.; Huang, J.; To, A. K. W.; Lai, J. H. C.; Xiao, P.; Wu, E. X.; Xu, J.; Chan, K. W. Y. CEST MRI Detectable Liposomal Hydrogels for Multiparametric Monitoring in the Brain at 3T. *Theranostics* **2020**, *10*, 2215−2228.
(127) Zhu, W.; Chu, C.; Kuddannaya, S.; Yuan, Y.; Walczak, P.; Singh, A.; Song, X.; Bulte, J. W. M. In Vivo Imaging of Composite Hydrogel Scaffold Degradation Using CEST MRI and Two-Color NIR Imaging. *Adv. Funct. Mater.* **2019**, *29*, 1903753.
(128) Kuddannaya, S.; Zhu, W.; Chu, C.; Singh, A.; Walczak, P.; Bulte, J. W. M. In Vivo Imaging of Allografted Glial-Restricted Progenitor Cell Survival and Hydrogel Scaffold Biodegradation. *ACS Appl. Mater. Interfaces* **2021**, *13*, 23423−23437.
(129) Lock, L. L.; Li, Y.; Mao, X.; Chen, H.; Staedtke, V.; Bai, R.; Ma, W.; Lin, R.; Li, Y.; Liu, G.; Cui, H. One-Component Supramolecular Filament Hydrogels As Theranostic Label-Free Magnetic Resonance Imaging Agents. *ACS Nano* **2017**, *11*, 797−805.
(130) Bagga, P.; Wilson, N.; Rich, L.; Marincola, F. M.; Schnall, M. D.; Hariharan, H.; Haris, M.; Reddy, R. Sugar Alcohol Provides Imaging Contrast in Cancer Detection. *Sci. Rep.* **2019**, *9*, 11092.
(131) Park, S. W.; Lai, J. H. C.; Han, X.; Leung, V. W. M.; Xiao, P.; Huang, J.; Chan, K. W. Y. Preclinical Application of CEST MRI to Detect Early and Regional Tumor Response to Local Brain Tumor Treatment. *Pharmaceutics* **2024**, *16*, 101.
(132) Xiao, P.; Huang, J.; Han, X.; Cheu, J. W. S.; Liu, Y.; Law, L. H.; Lai, J. H. C.; Li, J.; Park, S. W.; Wong, C. C. L.; Lam, R. H. W.; Chan, K. W. Y. Monitor Tumor pHe and Response Longitudinally during Treatment Using CEST MRI-Detectable Alginate Microbeads. *ACS Appl. Mater. Interfaces* **2022**, *14*, 54401−54410.

https://doi.org/10.1021/acsnano.4c05923
ACS Nano 2024, 18, 33775−33791

(133) Zhang, X.; Yuan, Y.; Li, S.; Zeng, Q.; Guo, Q.; Liu, N.; Yang, M.; Yang, Y.; Liu, M.; McMahon, M. T.; Zhou, X. Free-Base Porphyrins as CEST MRI Contrast Agents with Highly Upfield Shifted Labile Protons. *Magn. Reson. Med.* **2019**, *82*, 577−585.
(134) Anemone, A.; Capozza, M.; Arena, F.; Zullino, S.; Bardini, P.; Terreno, E.; Longo, D. L.; Aime, S. In Vitro and In Vivo Comparison of MRI Chemical Exchange Saturation Transfer (CEST) Properties between Native Glucose and 3-O-Methyl-D-glucose in a Murine Tumor Model. *NMR Biomed.* **2021**, *34*, No. e4602.
(135) Han, Z.; Zhang, S.; Fujiwara, K.; Zhang, J.; Li, Y.; Liu, J.; van Zijl, P. C. M.; Lu, Z. R.; Zheng, L.; Liu, G. Extradomain-B Fibronectin-Targeted Dextran-Based Chemical Exchange Saturation Transfer Magnetic Resonance Imaging Probe for Detecting Pancreatic Cancer. *Bioconjugate Chem.* **2019**, *30*, 1425−1433.
(136) Banerjee, S. R.; Song, X.; Yang, X.; Minn, I.; Lisok, A.; Chen, Y.; Bui, A.; Chatterjee, S.; Chen, J.; van Zijl, P. C. M.; McMahon, M. T.; Pomper, M. G. Salicylic Acid-Based Polymeric Contrast Agents for Molecular Magnetic Resonance Imaging of Prostate Cancer. *Chemistry* **2018**, *24*, 7235−7242.
(137) Di Gregorio, E.; Rosa, E.; Ferrauto, G.; Diaferia, C.; Gallo, E.; Accardo, A.; Terreno, E. Development of Cationic Peptide-Based Hydrogels Loaded with Iopamidol for CEST-MRI Detection. *J. Mater. Chem. B* **2023**, *11*, 7435−7441.
(138) Consolino, L.; Irrera, P.; Romdhane, F.; Anemone, A.; Longo, D. L. Investigating Plasma Volume Expanders As Novel Macromolecular MRI-CEST Contrast Agents for Tumor Contrast-Enhanced Imaging. *Magn. Reson. Med.* **2021**, *86*, 995−1007.
(139) Chen, Z.; Li, Y.; Airan, R.; Han, Z.; Xu, J.; Chan, K. W. Y.; Xu, Y.; Bulte, J. W. M.; van Zijl, P. C. M.; McMahon, M. T.; Zhou, S.; Liu, G. CT and CEST MRI Bimodal Imaging of the Intratumoral Distribution of Iodinated Liposomes. *Quant. Imaging Med. Surg.* **2019**, *9*, 1579.
(140) Yuan, Y.; Zhang, J.; Qi, X.; Li, S.; Liu, G.; Siddhanta, S.; Barman, I.; Song, X.; McMahon, M. T.; Bulte, J. W. M. Furin-Mediated Intracellular Self-Assembly of Olsalazine Nanoparticles for Enhanced Magnetic Resonance Imaging and Tumour Therapy. *Nat. Mater.* **2019**, *18*, 1376−1383.
(141) Tang, Y.; Xiao, G.; Shen, Z.; Zhuang, C.; Xie, Y.; Zhang, X.; Yang, Z.; Guan, J.; Shen, Y.; Chen, Y.; Lai, L.; Chen, Y.; Chen, S.; Dai, Z.; Wang, R.; Wu, R. Noninvasive Detection of Extracellular pH in Human Benign and Malignant Liver Tumors Using CEST MRI. *Front. Oncol.* **2020**, *10*, 578985.
(142) Jia, Y.; Wang, C.; Zheng, J.; Lin, G.; Ni, D.; Shen, Z.; Huang, B.; Li, Y.; Guan, J.; Hong, W.; Chen, Y.; Wu, R. Novel Nanomedicine with a Chemical-Exchange Saturation Transfer Effect for Breast Cancer Treatment In Vivo. *J. Nanobiotechnol.* **2019**, *17*, 1−14.
(143) Pavuluri, K.; Yang, E.; Ayyappan, V.; Sonkar, K.; Tan, Z.; Tressler, C. M.; Bo, S.; Bibic, A.; Glunde, K.; McMahon, M. T. Unlabeled Aspirin As an Activatable Theranostic MRI Agent for Breast Cancer. *Theranostics* **2022**, *12*, 1937−1951.
(144) Kombala, C. J.; Kotrotsou, A.; Schuler, F. W.; de la Cerda, J.; Ma, J. C.; Zhang, S.; Pagel, M. D. Development of a Nanoscale Chemical Exchange Saturation Transfer Magnetic Resonance Imaging Contrast Agent That Measures pH. *ACS Nano* **2021**, *15*, 20678−20688.
(145) Chen, M.; Chen, C.; Shen, Z.; Zhang, X.; Chen, Y.; Lin, F.; Ma, X.; Zhuang, C.; Mao, Y.; Gan, H.; Chen, P.; Zong, X.; Wu, R. Extracellular pH Is a Biomarker Enabling Detection of Breast Cancer and Liver Cancer Using CEST MRI. *Oncotarget* **2017**, *8*, 45759−45767.
(146) Jin, T.; Nicholls, F. J.; Crum, W. R.; Ghuman, H.; Badylak, S. F.; Modo, M. Diamagnetic Chemical Exchange Saturation Transfer (diaCEST) Affords Magnetic Resonance Imaging of Extracellular Matrix Hydrogel Implantation in a Rat Model of Stroke. *Biomaterials* **2017**, *113*, 176−190.
(147) Wang, R.; Wang, C.; Dai, Z.; Chen, Y.; Shen, Z.; Xiao, G.; Chen, Y.; Zhou, J. N.; Zhuang, Z.; Wu, R. An Amyloid-beta Targeting Chemical Exchange Saturation Transfer Probe for In Vivo Detection of Alzheimer's Disease. *ACS Chem. Neurosci.* **2019**, *10*, 3859−3867.
(148) Liu, G.; Moake, M.; Har-el, Y. E.; Long, C. M.; Chan, K. W. Y.; Cardona, A.; Jamil, M.; Walczak, P.; Gilad, A. A.; Sgouros, G.; van Zijl, P. C. M.; Bulte, J. W. M.; McMahon, M. T. In Vivo Multicolor Molecular MR Imaging Using Diamagnetic Chemical Exchange Saturation Transfer Liposomes. *Magn. Reson. Med.* **2012**, *67*, 1106−1113.
(149) Luo, J.; Abaci Turk, E.; Gagoski, B.; Copeland, N.; Zhou, I. Y.; Young, V.; Bibbo, C.; Robinson, J. N.; Zera, C.; Barth Jr, W. H.; Roberts, D. J.; Sun, P. Z.; Grant, P. E. Preliminary Evaluation of Dynamic Glucose Enhanced MRI of the Human Placenta During Glucose Tolerance Test. *Quant. Imaging Med. Surg.* **2019**, *9*, 1619−1627.
(150) Sebastiani, V.; Ricci, F.; Rubio-Viquiera, B.; Kulesza, P.; Yeo, C. J.; Hidalgo, M.; Klein, A.; Laheru, D.; Iacobuzio-Donahue, C. A. Immunohistochemical and Genetic Evaluation of Deoxycytidine Kinase in Pancreatic Cancer: Relationship to Molecular Mechanisms of Gemcitabine Resistance and Survival. *Clin. Cancer Res.* **2006**, *12*, 2492−2497.
(151) Smith, D. A.; Beaumont, K.; Maurer, T. S.; Di, L. Clearance in Drug Design. *J. Med. Chem.* **2019**, *62*, 2245−2255.
(152) Du, B.; Yu, M.; Zheng, J. Transport and Interactions of Nanoparticles in the Kidneys. *Nat. Rev. Mater.* **2018**, *3*, 358−374.
(153) Krause, W. Delivery of Diagnostic Agents in Computed Tomography. *Adv. Drug Delivery Rev.* **1999**, *37*, 159−173.
(154) Wahsner, J.; Gale, E. M.; Rodriguez-Rodriguez, A.; Caravan, P. Chemistry of MRI Contrast Agents: Current Challenges and New Frontiers. *Chem. Rev.* **2019**, *119*, 957−1057.
(155) Xie, A.; Hanif, S.; Ouyang, J.; Tang, Z.; Kong, N.; Kim, N. Y.; Qi, B.; Patel, D.; Shi, B.; Tao, W. Stimuli-Responsive Prodrug-Based Cancer Nanomedicine. *EBioMedicine* **2020**, *56*, 102821.
(156) Zha, S.; Liu, H.; Li, H.; Li, H.; Wong, K. L.; All, A. H. Functionalized Nanomaterials Capable of Crossing the Blood-Brain Barrier. *ACS Nano* **2024**, *18*, 1820−1845.
(157) Cook, A. B.; Decuzzi, P. Harnessing Endogenous Stimuli for Responsive Materials in Theranostics. *ACS Nano* **2021**, *15*, 2068−2098.
(158) El-Sawy, H. S.; Al-Abd, A. M.; Ahmed, T. A.; El-Say, K. M.; Torchilin, V. P. Stimuli-Responsive Nano-Architecture Drug-Delivery Systems to Solid Tumor Micromilieu: Past, Present, and Future Perspectives. *ACS Nano* **2018**, *12*, 10636−10664.
(159) Aafreen, S.; Feng, J.; Wang, W.; Liu, G. Theranostic Extracellular Vesicles: A Concise Review of Current Imaging Technologies and Labeling Strategies. *Extracell. Vesicles Circ. Nucleic Acids* **2023**, *4*, 107.
(160) Jayapaul, J.; Komulainen, S.; Zhivonitko, V. V.; Mares, J.; Giri, C.; Rissanen, K.; Lantto, P.; Telkki, V. V.; Schroder, L. Hyper-CEST NMR of Metal Organic Polyhedral Cages Reveals Hidden Diastereomers with Diverse Guest Exchange Kinetics. *Nat. Commun.* **2022**, *13*, 1708.
(161) Gao, Y.; Chu, C.; Jablonska, A.; Bulte, J. W. M.; Walczak, P.; Janowski, M. Imaging As a Tool to Accelerate the Translation of Extracellular Vesicle-Based Therapies for Central Nervous System Diseases. *Wiley Interdiscip. Rev.: Nanomed. Nanobiotechnol.* **2021**, *13*, No. e1688.
(162) Walker, S.; Busatto, S.; Pham, A.; Tian, M.; Suh, A.; Carson, K.; Quintero, A.; Lafrence, M.; Malik, H.; Santana, M. X.; Wolfram, J. Extracellular Vesicle-Based Drug Delivery Systems for Cancer Treatment. *Theranostics* **2019**, *9*, 8001.

https://doi.org/10.1021/acsnano.4c05923
ACS Nano 2024, 18, 33775−33791